Journal of Geodynamics 58 (2012) 44–61

Contents lists available at SciVerse ScienceDirect

Journal of Geodynamics

journal homepage: http://www.elsevier.com/locate/jog

Review

Geocenter motion and its geodetic and geophysical implications

Xiaoping Wu [a,*], Jim Ray [b], Tonie van Dam [c]

[a] Jet Propulsion Laboratory, California Institute of Technology, Pasadena, CA 91109, USA
[b] NOAA National Geodetic Survey, Silver Spring, MD 20910, USA
[c] University of Luxembourg, Luxembourg, Luxembourg

ARTICLE INFO

Article history:
Received 4 July 2011
Received in revised form 12 January 2012
Accepted 14 January 2012
Available online 28 January 2012

Keywords:
Geocenter motion
Satellite geodesy
Reference frame
Surface mass variation
Glacial isostatic adjustment

ABSTRACT

The horizontal transport of water in Earth's surface layer, including sea level change, deglaciation, and surface runoff, is a manifestation of many geophysical processes. These processes entail ocean and atmosphere circulation and tidal attraction, global climate change, and the hydrological cycle, all having a broad range of spatiotemporal scales. The largest atmospheric mass variations occur mostly at synoptic wavelengths and at seasonal time scales. The longest wavelength component of surface mass transport, the spherical harmonic degree-1, involves the exchange of mass between the northern and southern hemispheres. These degree-1 mass loads deform the solid Earth, including its surface, and induce geocenter motion between the center-of-mass of the total Earth system (CM) and the center-of-figure (CF) of the solid Earth surface. Because geocenter motion also depends on the mechanical properties of the solid Earth, monitoring geocenter motion thus provides an additional opportunity to probe deep into Earth's interior. Most modern geodetic measurement systems rely on tracking data between ground stations and satellites that orbit around CM. Consequently, geocenter motion is intimately related to the realization of the International Terrestrial Reference Frame (ITRF) origin, and, in various ways, affects many of our measurement objectives for global change monitoring. In the last 15 years, there have been vast improvements in geophysical fluid modeling and in the global coverage, densification, and accuracy of geodetic observations. As a result of these developments, tremendous progress has been made in the study of geocenter motion over the same period. This paper reviews both the theoretical and measurement aspects of geocenter motion and its implications.

Contents

* Corresponding author.
E-mail address: xp_wu@yahoo.com (X. Wu).

0264-3707/$ – see front matter © 2012 Elsevier Ltd. All rights reserved.
doi:10.1016/j.jog.2012.01.007

1. Introduction

The center-of-mass (CM) of the total Earth system, that is the solid Earth and its fluid envelope, is usually referred to as the geocenter (Petit and Luzum, 2010). The geocenter is used to describe Earth's motion in inertial space and serves as the orbital center for all Earth satellites. In this paper, the term "geocenter motion" is defined as the motion of the CM with respect to the center-of-figure (CF) of the solid Earth surface (e.g., Ray, 1999 and the contributions therein). (The reader should bear in mind that other conventions/definitions exist and are present in the literature.) Yet it is the solid Earth (and its CF origin) that actually moves within the reference frame if the origin is defined at CM. This is the convention that is generally recommended for most physical modeling, such as in the IERS Conventions (Petit and Luzum, 2010) for general relativistic formulations. Furthermore, the origin of the secular ITRF (Altamimi et al., 2007, 2011) is a long-term average of satellite CM realizations. In any case, the concept of relative motion is important because CM can only be observed from points fixed to the Earth's surface via geodetic satellite data, integrated over certain discrete time intervals.

Ever since the publication of the review article of Farrell (1972), geocenter motion has been recognized as a direct consequence of degree-1 ($n = 1$) surface or internal (Greff-Lefftz and Legros, 1997) loading and involves a special case of the load-induced deformation in the spherical harmonic domain. This unique, very long-wavelength component is important (critically so in many cases) for understanding global mass redistribution processes such as sea level rise, atmospheric and ocean circulation, present-day ice mass imbalance, continental hydrology, ocean tides, glacial isostatic adjustment (GIA), and geodynamic processes of the Earth's core and mantle (e.g., Stolz, 1976; Trupin et al., 1992; Dong et al., 1997; Greff-Lefftz and Legros, 1997, 2007; Watkins and Eanes, 1997; Chen et al., 1999; Blewitt et al., 2001; Wu et al., 2002; Blewitt and Clarke, 2003; Chambers et al., 2004; Klemann and Martinec, 2009; Greff-Lefftz et al., 2010).

Geocenter motion also depends on the elastic and viscoelastic properties of the solid Earth. The load-driven $n = 1$ displacement contributes to, but is not completely described by, the translational geocenter motion. For the complete spatial spectrum of global mass redistribution processes (including the $n = 1$ components), and to obtain additional information about the Earth's interior, it is crucial that geocenter motion and $n = 1$ deformation are understood and determined to a high degree of accuracy.

Geocenter motions have been modelled and analyzed using geophysical and climate models of ocean tides, atmospheric and ocean circulations, and land hydrology as well as GIA (e.g., Scherneck et al., 2000; Dong et al., 1997; Chen et al., 1999; Cretaux et al., 2002; Greff-Lefftz, 2000; Klemann and Martinec, 2009). The magnitudes of geocenter motions determined from these models at the different time scales are generally small. The amplitude is on the order of 1 cm due to diurnal and semi-diurnal ocean tides; a few mm due to the non-tidal annual hemispheric mass exchange of water and atmospheric mass separately; and less than 1 mm/yr at the secular time scale.

Many aspects of these environmental mass models are well constrained by observational data, in particular the tidal variations of the open ocean away from the coasts and polar areas. In most cases, however, the non-tidal predictions tend to be less reliable. By and large, the data assimilating or forward-fitting models are incomplete, non-unique, and highly uncertain over certain spatiotemporal domains due to poorly known driving forces, inaccurately modelled process dynamics and parameters, as well as poor input data coverage and accuracy. There is also a general lack of realistic uncertainty assessments for the models. As we enter the age of millimeter accuracy in geodesy, the use of models to estimate geocenter motion is not sufficiently precise for many modern geodetic applications.

Geocenter motion can also be directly observed. Observing geocenter motion is theoretically simple, i.e., tracking satellites orbiting around CM from stations located on Earth's surface. In reality, actual measurements of such small motions are very challenging due to the stringent consistency and accuracy requirements that must be provided by the tracking data themselves and the kinematic/dynamic modeling of the geodetic systems. In fact, measuring geocenter motion is at the forefront of high-precision global geodetic endeavors and has become a robust performance indicator for various geodetic techniques (Stolz, 1976; Vigue et al., 1992; Eanes et al., 1997; Watkins and Eanes, 1997; Pavlis, 1999; Bouille et al., 2000; Cretaux et al., 2002; Moore and Wang, 2003; Collilieux et al., 2009; Kang et al., 2009; Cheng et al., 2010; Rebischung and Garayt, 2010).

Another approach to observing geocenter motion was first recognized by Blewitt et al. (2001). The authors demonstrated the possibility of observing the $n = 1$ deformation and its annual variability using a set of globally distributed Global Positioning System (GPS) stations. Since that time, a new area of research involving inverse determination of geocenter motion has emerged (Wu et al., 2002, 2003; Blewitt and Clarke, 2003; Kusche and Schrama, 2005; Clarke et al., 2005, 2007; Lavallée et al., 2006). Unified approaches to combine satellite geocenter information and $n = 1$ deformation have also been studied and carried out (Lavallée et al., 2006; Fritsche et al., 2010).

The launch of the Gravity Recovery and Climate Experiment (GRACE) mission in 2002 (Tapley et al., 2004) spurred a requirement for accurate measurements of geocenter motion and the underlying $n = 1$ surface mass transport. GRACE provides, for the first time, a near-global monitoring capability for surface mass transport. However, GRACE alone is not capable of observing the degree-1 mass redistribution. GRACE's rich data stream, global coverage, and high-accuracy have greatly stimulated research efforts to determine geocenter motion incorporating multiple and interdisciplinary data sets (Davis et al., 2004; Wu et al., 2006, 2010a,b; Munekane, 2007; Swenson et al., 2008; Jansen et al., 2009; Rietbroek et al., 2009, in press-a, in press-b).

The requirement for millimeter precision in many applications of geodetic observations means that the effect of geocenter motion can no longer be ignored. For example, one important geophysical/climate change implication of geocenter motion concerns the accurate determination of mean sea level (MSL) rise and its causes. The primary modern geodetic technique for measuring MSL is satellite altimetry, which provides far better spatial coverage than traditional tide gauge measurements. The satellite-based measurement is referenced in the CM frame over the long-term and is often denoted as the absolute sea level. However, to study geophysical sources of sea level rise, such as thermal expansion of the oceans or

the addition of fresh water to the oceans, volumetric changes of the ocean with respect to the mean ocean floor are required (Blewitt, 2003). In this case, to convert altimetric measurements of MSL to a volume change, a correction of the geocenter motion with respect to the mean ocean floor has to be applied.

Another important aspect of geocenter motion relates to the interpretation and application of the ITRF. Because the ITRF is optimally derived from combinations of all space geodetic solutions, its datum definition and realization are intimately related to the geocenter and the geocenter motion with respect to the surface of the Earth. Currently, the ITRF assumes linear motions for ground stations (except for occasional discontinuities). As a result, the ITRF coordinate origins are theoretically defined at the long-term mean CM rather than at any quasi-instantaneous CM. In fact, over subsecular time scales, the ITRF origin is approximately located at a point with a fixed offset from CF with no motion between them (Blewitt, 2003; Dong et al., 2003; Collilieux et al., 2009; and see below). For consistency, any geodetic tracking system having its coordinate origin fixed at the origin of the ITRF, therefore, would need corrections for instantaneous geocenter motions if they or the equivalent $n = 1$ gravitational coefficients are not explicitly estimated. Prominent examples of these systems include ocean and ice altimetry mission series such as TOPEX/Poseidon, Jason, ICESat, and CryoSat, as well as any other spacecraft position determinations that use the precise point positioning technique (Zumberge et al., 1997; Haines et al., 2004) with Global Navigation Satellite Systems (GNSS) (including GPS) tracking.

Independently determined geocenter motion time series can be used to correct various geodetic coordinate time series to provide a globally unified displacement time series in the instantaneous CM frame. Alternatively, ITRF input data time series and results contain geocenter motion information that can be used to (1) determine geocenter motion at sub-secular time scales directly (Collilieux et al., 2009) or to (2) compare with global fluid models and independent geocenter motion estimates to validate the accuracies of the ITRF data (Collilieux et al., 2009) and origin realization (Wu et al., 2011).

Clearly a precise knowledge of geocenter motion is fundamental for interpreting geodetic observations and for connecting observations from orbiting satellites to their ground based tracking stations. In this paper, we present a review of the state of the art in geocenter motion theory, observations and modeling. Section 2 provides a review of the theoretical aspects of geocenter motion. In Section 3, we review the geophysical causes of geocenter motion. Section 4 assesses in detail the relationship between the geocenter and the ITRF and sea level observations. In Section 5, we discuss methodology and progress in observing geocenter motion due to surface mass transport and GIA. Finally we present a discussion in Section 6 on the prospects for improving geocenter modeling and theoretical developments and conclude in Section 7.

2. Theory of geocenter motion due to a degree-1 load

Earth's surface layer, consisting of the atmosphere, hydrosphere, and cryosphere, undergoes constant dynamic changes resulting in the temporal redistribution of mass. (Processes in Earth's deep interior, apart from GIA, are not considered in detail here due to a lack of research and data constraints, long time scales, and their (probably) small amplitude. However, any surface expressions of topography or geopotential due to internal mass movements could be incorporated into the theory here using a similar formalism such as exists for exterior fluids.) Compared to Earth's radius, the thickness of the surface layer is relatively thin so that vertical mass redistributions can generally be ignored. Then the horizontal mass redistribution can be represented by (incremental) surface mass density (with respect to a reference epoch) and expressed as a sum of spherical harmonic series (e.g., Wahr et al., 1998):

$$\sigma(\vartheta,\varphi,t)=\frac{dM}{dS}=\rho_w h(\vartheta,\varphi,t)=\sum_{n=1}^{\infty}\sum_{m=0}^{n}\sum_{q=c,s}\sigma_{nmq}(t)Y_{nmq}(\vartheta,\varphi), \tag{1}$$

where M and S are mass and surface area. The variable ρ_w is the reference density of water and h is equivalent water thickness. The variables σ_{nmq} and Y_{nmq} are real-valued and normalized spherical harmonic coefficients and functions, respectively, defined using the standard geodetic convention (Lambeck, 1988). Index $q = c,s$ indicates $\cos(m\varphi)$ or $\sin(m\varphi)$ coefficients and functions. The degree-0 term drops out of the summation because the total mass in the surface layer is considered constant.

In a reference frame with the coordinate origin defined as the instantaneous center of mass of the solid Earth (CE), the position vector of CE is $r_{ce} = 0$. The position of the center of mass of any body, such as the incremental load in the surface layer, is defined as

$$\begin{aligned}\mathbf{r}_l &= \frac{1}{M_l}\iint[x\hat{\mathbf{e}}_x+y\hat{\mathbf{e}}_y+z\hat{\mathbf{e}}_z]\sigma a^2\sin\vartheta d\vartheta d\varphi\\ &= \frac{4\pi a^3}{\sqrt{3}M_l}(\sigma_{11c}\hat{\mathbf{e}}_x+\sigma_{11s}\hat{\mathbf{e}}_y+\sigma_{10c}\hat{\mathbf{e}}_z),\end{aligned} \tag{2}$$

where M_l and a are the load mass and radius of Earth, respectively; orthonormal properties of the spherical harmonic functions have been used. Equation (2) demonstrates that only $n = 1$ coefficients are associated with the position (and movement) of the center of mass. Note that $M_E\mathbf{r}_{cm} = M_s\mathbf{r}_{ce} + M_l\mathbf{r}_l = M_l\mathbf{r}_l$, where M_s is the mass of the solid Earth. From this equation and using (2), the incremental position of CM in the CE frame is,

$$\mathbf{r}_{cm}=\frac{M_l}{M_E}\mathbf{r}_l=\frac{4\pi a^3}{\sqrt{3}M_E}(\sigma_{11c}\hat{\mathbf{e}}_x+\sigma_{11s}\hat{\mathbf{e}}_y+\sigma_{10c}\hat{\mathbf{e}}_z), \tag{3}$$

where M_E is the mass of the total Earth system including the surface fluid layer. Equation (3) expresses the relative motion of CM with respect to CE driven by the $n = 1$ surface load variation. Changes in surface load also deform the underlying solid Earth including its surface, where all geodetic stations are located.

Now we introduce the concept of CF whose motion is equivalent to the integral average motion of the entire surface (Trupin et al., 1992):

$$\mathbf{r}_{cf}=\frac{1}{4\pi}\iint\mathbf{r}(\vartheta,\varphi)\sin\vartheta d\vartheta d\varphi, \tag{4}$$

where $\mathbf{r}_{cf}$ is the incremental position or displacement of CF from the reference epoch position and $r(\vartheta,\varphi)$ is the displacement of a point on the surface of the solid Earth. Since a geodetic network has only a finite number of sites, N, the incremental (geometric) center of network (CN) is also used to describe the translational motion of the network:

$$\mathbf{r}_{cn}=\frac{1}{N}\sum_{i=1}^{N}\mathbf{r}_i. \tag{5}$$

The geometry of the various centers is illustrated in Fig. 1. For real tracking networks, relative motions between CF and CN occur due to non-uniform surface coverage and peculiar local motions at individual stations. Such spurious contributions to apparent geocenter motion measurements have been termed "network effect" (see, for example, Collilieux et al. (2009), where approaches to mitigate the effect were also studied).

To learn about load-induced deformation and geocenter motion, we have to distinguish the solid Earth's responses to loading at two different time scales.

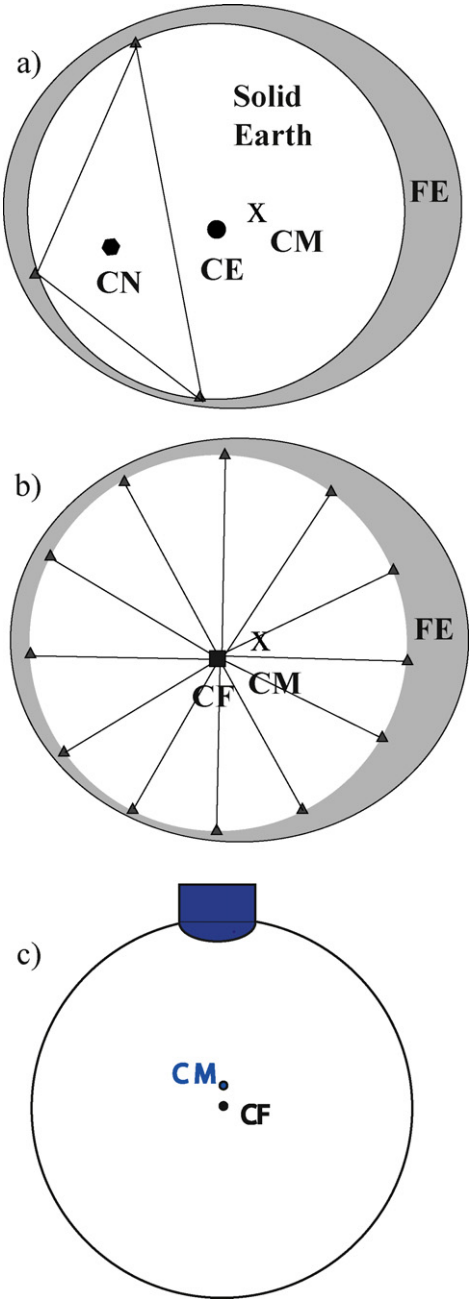

Fig. 1. Simplified illustration of the different reference frames used in geodesy. The solid circle in a) represents the center of mass of the solid Earth (CE) while the cross represents the center of mass of the total Earth (CM), being the solid Earth plus the surface mass system in the fluid envelope (FE). The center of network (CN, black hexagon) is different from both CE and CM in the extreme case of only three stations; b) shows the theoretical situation of having geodetic sites evenly spaced over the Earth's entire surface (including the oceans) for which CF = CE; (from Tregoning and van Dam, 2005); c) illustrates the exaggerated deformation of the solid Earth, its surface, and CF under loading.

2.1. Elastic Earth deformation

Over time scales from sub-daily to decadal, the solid Earth behaves elastically under loading and unloading. The elastic load deformation theory outlined by Farrell (1972) for the spherically symmetric, stratified, and non-rotating Earth is fairly adequate and as a result has been used widely within the geodetic community. The linearized governing equations are the conservation of linear momentum:

$$\rho\partial_t^2\mathbf{s} = \nabla\cdot\mathbf{T} + g\nabla\cdot(\rho\mathbf{s})\hat{\mathbf{e}}_r - \rho\nabla\phi - \nabla(\rho g\mathbf{s}\cdot\hat{\mathbf{e}}_r), \tag{6}$$

Poisson's equation:

$$\nabla^2\phi = -4\pi G\nabla\cdot(\rho\mathbf{s}), \tag{7}$$

and the elastic constitutive relation or Hooke's law:

$$\mathbf{T} = \lambda(\nabla\cdot\mathbf{s})\mathbf{I} + \mu[\nabla\mathbf{s} + (\nabla\mathbf{s})^{\mathrm{T}}], \tag{8}$$

as well as the boundary conditions of a unit point mass load problem. $\mathbf{s}$, $\mathbf{T}$, and ϕ are the displacement, incremental Cauchy stress, and perturbation in the gravitational potential, respectively. ρ and g are the equilibrium density and gravity values. G is the gravitational constant. λ and μ are Lamé parameters. $\mathbf{I}$ is the second rank identity tensor. The ijth element of the displacement gradient is defined as $\partial s_j/\partial x_i$.

After Fourier transforming Equations (6–8), the dynamic equations are solved using spheroidal vector spherical harmonic functions. For the problem of loading on a spherical and non-rotating Earth, the toroidal components are completely decoupled in the governing equations and vanish in the solution without any tangential stress forcing at the surface. For point load problems at frequencies lower than those of the Earth's free oscillations, the equations and solutions do not depend on order m or frequency. Thus, the coefficients of the vector functions depend only on the radial coordinate r and are governed by a set of ordinary differential equations and boundary conditions decoupled for each angular degree n:

$$\frac{d\mathbf{Y}_n(r)}{dr} = \mathbf{A}_n(r)\mathbf{Y}_n(r) \tag{9}$$

where $\mathbf{Y}_n = (U_n, V_n, N_n, T_n, \Phi_n, Q_n)^{\mathrm{T}}$ contains radial and lateral displacements, normal and tangential stresses, gravitational potential, and potential gradient. These equations can then be solved numerically, from the center of the realistically stratified Earth to the surface, with unknown coefficients of solutions determined by the boundary conditions.

The $n = 1$ case, however, is special. Here, the boundary condition equations are not linearly independent as would facilitate a unique solution. Physically, the way the problem is posed allows an arbitrary uniform translation of the solid Earth without any violation of the equations and boundary conditions. In other words, the coordinate origin of the problem has not been explicitly specified. An extra equation can be used to determine the amount of the translational motion by setting the coordinate origin either at CM or CE. Although no confusion can arise mathematically by this arrangement, there have been ambiguities in the historical literature semantics as to the definition of the chosen origin. The phrases "center of mass of an undeformed Earth" and "center of mass of a deforming (or deformed) Earth" have been used to describe CE. In addition, the phrase "center of mass of a deformed Earth" has occasionally been used to describe CM. Since the Earth is undergoing constant change, and a reference frame origin has to be specified at all time epochs, it is conceptually much clearer to call the origin the instantaneous CM or CE, and the coordinates of CM or CE will be zero for all time in the respective frame.

The total response of the Earth to a real load variation at the surface can be computed by convolving the load with the point load responses, i.e., Green's functions. The Green's functions depend on the load Love numbers, the dimensionless ratios of the solid Earth responses to the forcing gravitational potential. Depending on the origin choice of CM or CE, the $n = 1$ load Love numbers will have different values that are related to one another through the

following simple relationships (Greff-Lefftz and Legros, 1997; Blewitt, 2003):

$$h_1'^{ce} = 1 + h_1'^{cm}, \quad k_1'^{ce} = 1 + k_1'^{cm}, \quad l_1'^{ce} = 1 + l_1'^{cm}, \tag{10}$$

where $h_1'^{ce}, k_1'^{ce}, l_1'^{ce}$ are the $n=1$ vertical, potential, and tangential load Love numbers respectively when the coordinate origin is defined at CE; and $h_1'^{cm}, k_1'^{cm}, l_1'^{cm}$ are the Love numbers in the CM frame. It can be shown that $k_1'^{ce} = 0$ because the solid Earth cannot have an $n=1$ potential in this frame. Blewitt (2003) also derives a more general form of these relationships using load Love numbers defined in different coordinate systems including those in the CF frame. The $n>1$ load Love numbers, on the other hand, are invariant to the choice of the coordinate origin.

Using these observations, many geodetic signatures can be readily expressed as functions of the surface load and the load Love numbers. For example, it is customary for satellite gravity missions to adopt the CM frame, where the incremental gravitational geoid height becomes:

$$N^e = \sum_{n=2}^{\infty}\sum_{m=0}^{n}\sum_{q=c,s}\frac{4\pi a^3}{M_E(2n+1)}(1+k_n')\sigma_{nmq}Y_{nmq}. \tag{11}$$

The $n=1$ terms drop out because $k_1'^{cm} = -1$ reflecting the simple fact that the degree-1 effect of the surface load variation is balanced by that of the solid Earth mass redistribution in this frame. In other words, there can be no $n=1$ gravitational potential for the Earth system when the origin is defined at its center of mass. As another example, depending on the frame, the surface displacement due to elastic deformation is:

$$\mathbf{r}^e = \frac{4\pi a^3}{M_E}\sum_{n=1}^{\infty}\sum_{m=0}^{n}\sum_{q=c,s}\frac{\sigma_{nmq}}{2n+1} \times \left[h_n' Y_{nmq}\hat{\mathbf{e}}_r + l_n'\left(\partial_\vartheta Y_{nmq}\hat{\mathbf{e}}_\vartheta + \frac{1}{\sin\vartheta}\partial_\varphi Y_{nmq}\hat{\mathbf{e}}_\varphi\right)\right]. \tag{12}$$

In the CE frame, using (3) and substituting (12) into (4), the geocenter motion caused by present-day surface mass change is:

$$\mathbf{r}_{gc}^e = \mathbf{r}_{cm}^e - \mathbf{r}_{cf}^e = \frac{4\pi a^3}{\sqrt{3}M_E}\left(1 - \frac{h_1'^{ce} + 2l_1'^{ce}}{3}\right) \times \left(\sigma_{11c}\hat{\mathbf{e}}_x + \sigma_{11s}\hat{\mathbf{e}}_y + \sigma_{10c}\hat{\mathbf{e}}_z\right), \tag{13}$$

where $\mathbf{r}_{cm}^e$ is the displacement of CM due to active surface mass redistribution, and $\mathbf{r}_{cf}^e$ is the displacement of CF due to elastic deformation caused by the active redistribution.

2.2. Viscoelastic Earth deformation

Over longer periods (10^3–10^6 years), the solid Earth behaves more like a linear Maxwell viscoelastic body. Today the Earth continues to respond to the massive late-Pleistocene deglaciation events that occurred thousands of years ago. At present, the viscous rebound (GIA) signatures appear as constant time rates of change such as geocenter velocity, uplift and geoid change rates. These must be distinguished from present-day surface mass trend (PDMT) signatures that are also measured by modern geodetic techniques.

For a Maxwell viscoelastic rheology, the constitutive relation is:

$$\dot{T}_{ij} + \left(\frac{\mu}{\nu}\right)\left(T_{ij} - \frac{1}{3}T_{kk}\delta_{ij}\right) = 2\mu\dot{E}_{ij} + \lambda\dot{E}_{kk}\delta_{ij}, \tag{14}$$

where double indices imply summations. E is the strain tensor, and ν is the viscosity. It can be shown that in the Laplace transform domain, the constitutive relation retains the form of Hooke's law in (8), however, the Lamé parameters become functions of frequency, s. Therefore, the viscoelastic equations can be solved using the Correspondence Principle, i.e. we can now employ the elastic solutions to the Laplace transformed version of the corresponding viscoelastic equations (Vermeersen et al., 1996). The time domain response can then be found by performing the inverse Laplace transform (Wu, 1978). Similar to the previous section, the load Love numbers and Green's functions are used to describe Earth's responses to an impulse point load (Peltier, 1974). Here, in the frequency domain, a generic s-domain Love number θ_n is first expanded as a Laurent series with first order poles, and the corresponding time domain load Love number is a sum of relaxation modes:

$$\theta_n(s) = \theta_n^E + \sum_j \frac{r_j}{s+s_j}, \quad \theta_n(t) = \theta_n^E\delta(t) + \sum_j r_j e^{-s_j t}H(t), \tag{15}$$

where θ_n^E is the elastic load Love number. s_j are the inverse relaxation times of the modes and can be found as roots to the secular determinant equation of the free problem with the homogeneous boundary condition. r_j are the strengths of the modes and can be determined by complex contour integration using the residue theorem. $\delta(t)$ and $H(t)$ are the Dirac delta and Heaviside step functions, respectively. By convolving the spatiotemporal distribution of the load with the Green's functions, we can derive the Earth responses (e.g., Han and Wahr, 1995). The viscoelastic theory also includes an elastic component in (15). This factor is important for modeling historical records, but does not affect the current GIA signatures that are due to historical deglaciation. Finally, the GIA-induced geoid trend and surface velocity can be written, respectively, as:

$$\dot{N}^v = \sum_{n=2}^{\infty}\sum_{m=0}^{n}\sum_{q=c,s}\frac{4\pi a^3}{M_E(2n+1)}\dot{\sigma}_{nmq}^{v,k}Y_{nmq}, \tag{16}$$

and

$$\dot{\mathbf{r}}^v = \frac{4\pi a^3}{M_E}\sum_{n=1}^{\infty}\sum_{m=0}^{n}\sum_{q=c,s}\frac{1}{2n+1} \times \left[\dot{\sigma}_{nmq}^{v,h}Y_{nmq}\hat{\mathbf{e}}_r + \dot{\sigma}_{nmq}^{v,l}\left(\partial_\vartheta Y_{nmq}\hat{\mathbf{e}}_\vartheta + \frac{1}{\sin\vartheta}\partial_\varphi Y_{nmq}\hat{\mathbf{e}}_\varphi\right)\right], \tag{17}$$

where

$$\dot{\sigma}_{nmq}^{v,i} = \sum_j(-s_{nj})r_{nj}^i\int_{-\infty}^{t}\sigma_{nmq}(\tau)e^{s_{nj}(\tau-t)}d\tau, \tag{18}$$

and the superscript i can be either k, h, or l for potential, vertical, or horizontal coefficients.

As with the elastic case, the $n=1$ case is again different from the other angular degrees. Specifically, the M0 mode and the G mode associated with density contrasts across the surface and the inner/outer core boundary do not exist and only one viscoelastic mode exists for each viscoelastic interface (Greff-Lefftz and Legros, 1997). Such GIA-induced deformation, however, only causes the CM to move with respect to the CE by a tiny amount (0.04 mm/yr) at present. This is due to the fact that the historical forcing does not involve any active change in the present-day surface load except the equilibrium passive redistribution of oceanic water mass in response to the changing geoid and crust (Klemann and Martinec, 2009). As a result, the relations (10) still hold for the case of the viscoelastic Earth. In other words, there is no difference between the viscous components of any load Love number in the CM and CE frames that have negligible motion relative to each other as a result of the impulse load forcing. Therefore, in the CE frame, $\dot{\mathbf{r}}_{cm}^v \approx 0$ and substituting (17) into (4), we obtain GIA-induced geocenter

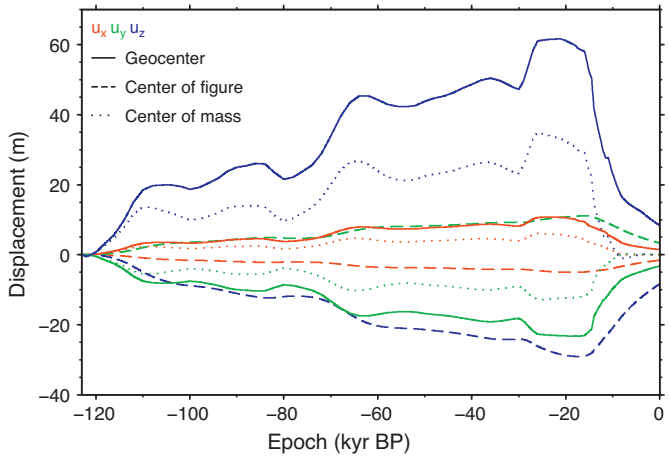

Fig. 2. Evolution of coordinate components of geocenter motion, CM and CF, in the CE frame as functions of time during the last glacial cycle. The loading model is ICE-5G. The Earth rheological profile LM+ is used, which assumes a 90-km thick lithosphere, an upper-mantle viscosity of 5×10^{20} Pa s, and a lower-mantle viscosity of 1×10^{22} Pa s.

Adapted from Klemann and Martinec (2009).

velocity:

$$\dot{\mathbf{r}}^{v}_{cm} - \dot{\mathbf{r}}^{v}_{cf} = -\dot{\mathbf{r}}^{v}_{cf} = -\frac{4\pi a^3}{3\sqrt{3}M_E} \times \left[(\dot{\sigma}^{v,h}_{11c} + 2\dot{\sigma}^{v,l}_{11c})\hat{\mathbf{e}}_x + (\dot{\sigma}^{v,h}_{11s} + 2\dot{\sigma}^{v,l}_{11s})\hat{\mathbf{e}}_y + (\dot{\sigma}^{v,h}_{10c} + 2\dot{\sigma}^{v,l}_{10c})\hat{\mathbf{e}}_z\right], \quad (19)$$

which, according to (18), depends on ice history and Earth rheology through the relaxation mode parameters. Although the current CM–CE motion due to historical deglaciation is tiny and is neglected here, it is possible to include it either as a part of PDMT (Wu et al., 2010b) or (preferably) GIA.

Recently, a time differencing and spectral-finite element approach to the initial/boundary value viscoelastic problem in the time domain has been applied to model the $n = 1$ GIA deformation (Klemann and Martinec, 2009). Both the modal and time differencing approaches suggest that late Pleistocene deglaciation events drive a significant amount of historical and present-day geocenter motion. The magnitude and direction of this geocenter motion depend strongly on lower-mantle viscosity and deglaciation history, and to a lesser extent, on upper-mantle viscosity and lithospheric thickness (Greff-Lefftz, 2000; Klemann and Martinec, 2009).

Fig. 2 shows the displacements of CM, CF and geocenter motion (CM–CF) during the last glacial cycle in the CE frame using the ICE-5G (Peltier, 2004) loading model and the LM+ (Klemann and Martinec, 2009) Earth rheology profile. Dependences of current GIA-induced geocenter velocity on Earth rheology and deglaciation history are shown, respectively, in Figs. 3 and 4. Historical geocenter motion due to $n = 1$ internal load-induced deformation has also been studied over even longer time scales using the Maxwell viscoelastic theory (Greff-Lefftz and Legros, 1997; Greff-Lefftz et al., 2010).

Here we conclude the theoretical survey. We have presented the theoretical development of geocenter motion for both elastic and viscoelastic Earth models. Both developments are necessary as the total observed present-day secular trend in geocenter is the sum of a PDMT and a GIA component. Specifically, the secular geocenter motion takes the form of the time derivative of Equations (13) plus (19).

3. Geophysical causes

3.1. Seasonal and interannual surface mass transport

External energy, i.e. heating from the Sun, drives the horizontal redistribution of continental water, oceanic, and atmospheric mass at the Earth's surface. These mass redistributions cause significant seasonal and interannual geocenter motion with amplitudes of a few mm. Snow and water over continents are the largest contributors to geocenter motion as compared to the atmosphere and the oceans. Further, there is a clear annual cycle in the pattern of hemispheric water mass exchange, with the northern hemisphere having more mass during the northern hemisphere winter.

The contributions of continental hydrology, oceans, and atmosphere have been studied using geophysical models (Dong et al., 1997; Chen et al., 1999; Bouille et al., 2000; Cretaux et al., 2002; Moore and Wang, 2003; Feissel-Vernier et al., 2006; Collilieux et al., 2009). Although many of the component models are incomplete and not well constrained by data, the predicted seasonal geocenter motions from the models tend to agree reasonably well with geodetic observations. However, an accurate assessment of the contributions of polar ice sheets is largely missing from the models. In addition, the long-term model performances over the regions covered by observations remain highly uncertain.

The GRACE mission has contributed significantly to our knowledge of the long-wavelength surface-water mass transport at seasonal time scales and beyond. Unfortunately, GRACE does not capture the degree-1 effects. In the CM frame, the $n = 1$ terms in (11) all vanish because $k_1^{cm} = -1$. In reality, the longest wavelength components of the global surface mass variation (σ_{1mq}) will not be zero, and are critical for accurate assessments of geographical water mass budgets. For example, let's determine the impact of adding 1 mm geocenter motion (or the equivalent $n = 1$ surface mass variation) to the geographical water mass budget determined from GRACE data. Table 1 shows the mean equivalent change in annual water thicknesses over various geographic regions due to this 1 mm geocenter motion. The values in the table can be applied to both amplitude and trend computations. The estimated effects of water mass change due to the unobserved geocenter motion in GRACE are non-negligible. Therefore, to monitor the complete spatial spectrum of water mass redistribution, geocenter motion has to be measured to sufficient accuracy to supplement the GRACE data. On the other hand, as we shall see in Section 5, GRACE's $n \geq 2$ global gravity measurements can also contribute greatly to the determination of σ_{1mq} when combined with other data.

Table 1
Effects of 1 mm geocenter motion component on GRACE mass change determination.

Region	Mean water thickness (mm)			Mass (gigaton)		
	GX	GY	GZ	GX	GY	GZ
Global ocean	−0.46	−0.26	−0.51	−173	−95	−190
Ocean (±66°)	−0.5	−0.26	−0.62	−173	−90	−215
Arctic ocean	0.1	−0.02	5.1	0.9	−0.3	70
Antarctica	0.04	0.38	−5.1	0.5	5	−69
Greenland	1.1	−1.0	5.0	2.5	−2.2	11

GRACE's mass budget estimate requires a complete surface mass variation spectrum including the degree-1 coefficients, which are not measured by the mission science data system but supplemented using equivalent geocenter motion estimates. The values in the table show net mean equivalent annual water thicknesses and mass over geographic regions due to including degree-1 coefficients that correspond to 1 mm geocenter motion along the coordinate axes. The same values show time rates of change in the mean thickness or mass (mm/yr or gigaton/yr) due to degree-1 trends that correspond to 1 mm/yr geocenter velocity. The table can also be used to propagate uncertainties of geocenter motion estimates into geographical mass budget estimates.

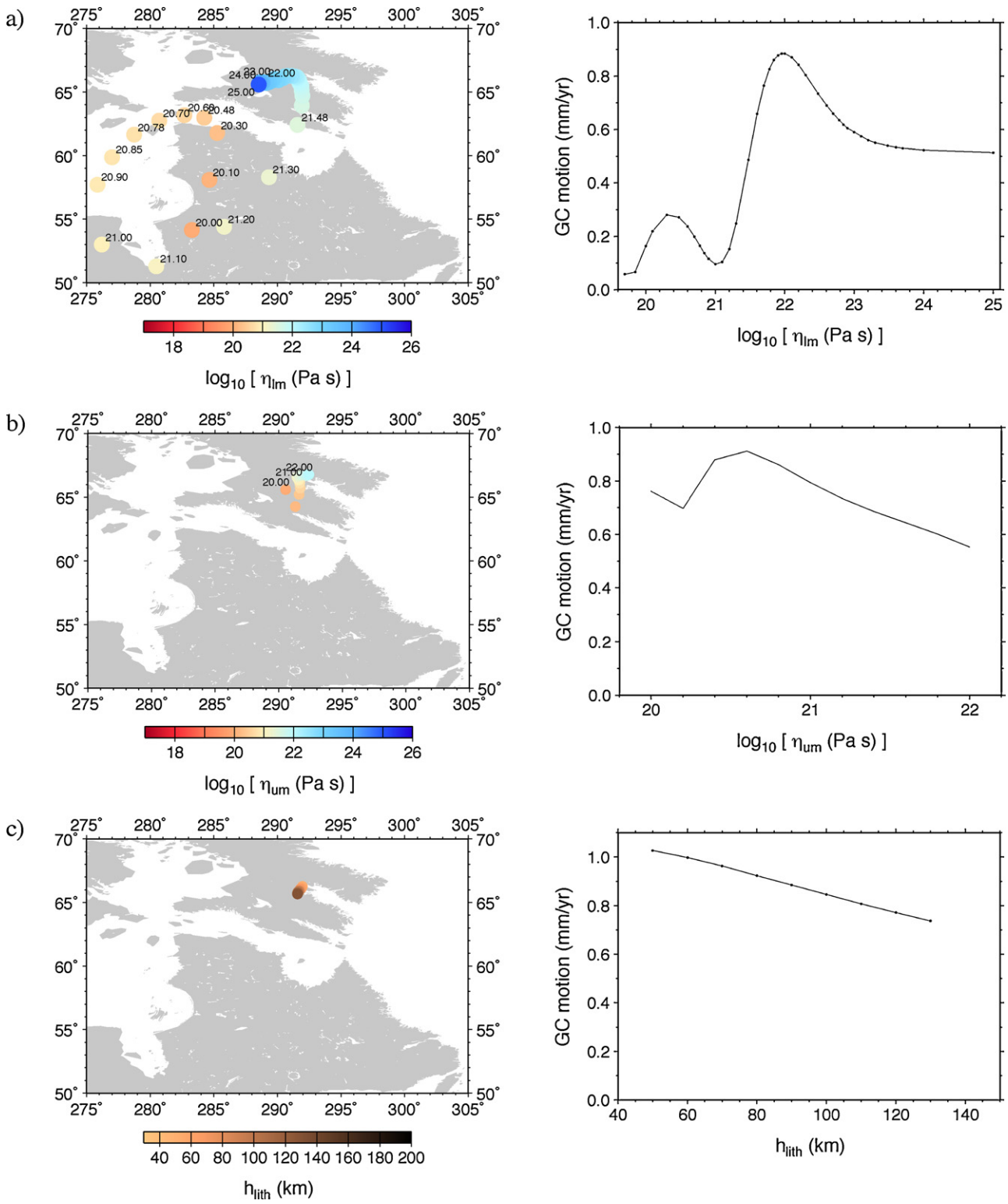

Fig. 3. Dependence of current (negative) geocenter velocity on individual Earth-model parameters. The reference values of ICE-5G and LM+ are used for unperturbed parameters. a) Velocities for different lower-mantle viscosities, b) velocities for different upper-mantle viscosities, c) velocities for different lithospheric thicknesses. Left panels show the directions of CF velocity relative to CM (the negative geocenter velocity) projected onto Earth's surface. Right panels show their amplitudes.
From Klemann and Martinec (2009).

3.2. Non-seasonal mass transport

Ocean tides, which span the spectrum from the semi-diurnal band to long periods up to 18.6 years, cause water mass redistributions that have attracted the attention of load deformation theorists since very early on (e.g., Farrell, 1972). The induced semi-diurnal and diurnal geocenter motions have amplitudes of sub-mm to a few mm per tide (Watkins and Eanes, 1997). All

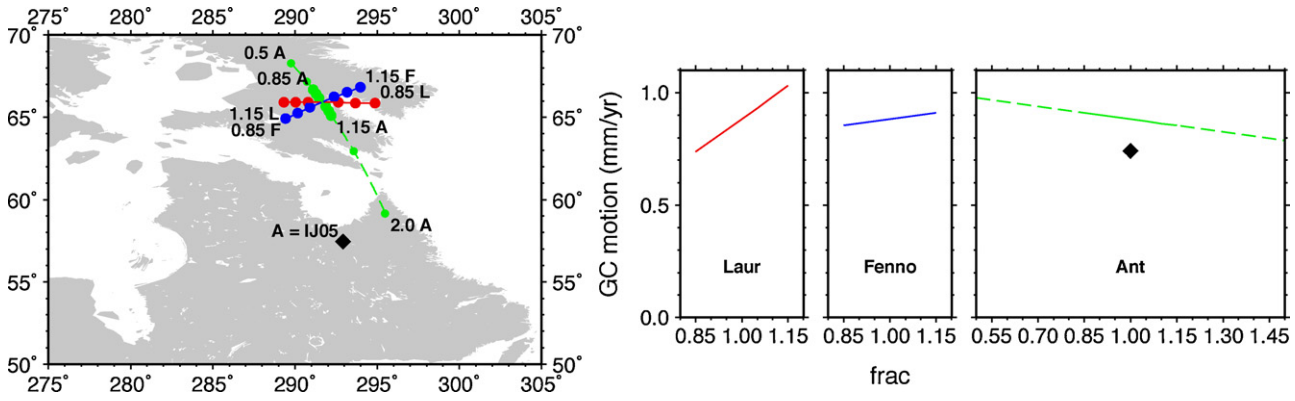

Fig. 4. Dependence of current (negative) geocenter velocity on loading scenarios using the LM+ rheology profile and different load fractions of ICE-5G where the total mass is not conserved. Left and right panels are like those in Fig. 3. Dashed green denotes motions due to the extended variations of ICE-5G from 0.5 to 2 for Antarctica and the diamond indicates the velocity when ICE-5G in Antarctica is replaced by IJ05 (Ivins and James, 2005).
From Klemann and Martinec (2009).

together the tidal contributions to geocenter motion can sum to about 1 cm (see the Ocean Tide Loading Service website at http://www.oso.chalmers.se/~loading/cmc.html).

The geocenter motion for the long-period tides are much smaller, usually less than 0.5 mm for the individual terms but these may also not be entirely negligible (Scherneck et al., 2000; Cretaux et al., 2002). Ocean tides measured by the TOPEX/Jason altimeter mission series, within the ±66° latitude-band, have successfully contributed to the improvement of data-assimilated hydrodynamic ocean tide models. They have been used to compute the induced deformation as well as geocenter motion (Scherneck et al., 2000). Although many modern global ocean tide models cover the Arctic and Southern Oceans, the accuracies there remain doubtful due to the limited observations in these remote regions. Accurately determined geocenter motion can thus potentially add to our knowledge of global ocean tides.

The consideration of tides within the atmosphere is currently restricted to the diurnal S1 and semi-diurnal S2 thermally driven modes. The IERS Conventions (Petit and Luzum, 2010) recommend the pressure tide model of Ray and Ponte (2003), for which the corresponding geocenter motion is given. Variations reach the level of about 1 mm, with the greatest effects occurring near the equatorial plane where the solar forcing is greatest.

According to the IERS Conventions, geodetic data analyses should account for tidal variations using the recommended models a priori in the station displacement of all techniques and in the geopotential and geocenter motion for satellite tracking observations. Consequently, the measurement results should be free of these tidal geocenter motions to within the accuracy of the models themselves.

In addition to these tidal effects, daily or sub-daily non-tidal atmospheric, oceanic, and hydrological activities can also induce geocenter motion. Among those, only the atmospheric circulation has been studied with the conclusion that the amplitudes here are generally very small (de Viron et al., 2005). The contribution to geocenter motion by the global vegetation biomass is even smaller with amplitudes on the order of a few tens of micrometers (Rodell et al., 2005).

Within the interior of the Earth, the Slichter elasto-gravitational normal modes involve translational oscillations of the inner core. If excited, these modes can generate geocenter motion at periods around 4–5 h. The detection of the Slichter triplet is still being debated (Smylie et al., 1993; Hinderer et al., 1995), possibly due to a limited signal-to-noise ratio. Nonetheless, the amplitudes of the geocenter motion due to the Slichter modes will be small (<0.1 mm) (Greff-Lefftz and Legros, 2007). Core boundary pressure variations over decadal time scales are another possible internal loading mechanism that might drive geocenter motion. This mechanism is estimated to contribute to geocenter motion at the level of ~0.3 mm (Greff-Lefftz and Legros, 2007).

Earth's deep interior remains a major scientific frontier where many processes and parameters are not known with sufficient certainty. Therefore, it is not clear how realistic the orders of magnitude of the above estimates are. In any event, geocenter motion of this magnitude could be significant. Therefore, the core pressure variation processes should be studied further.

3.3. Long-term mass transport processes

Thus far in this Section, we have focused on geocenter motions driven by surface mass loading at elastic time scales. The most significant surface mass transport is the dramatic late-Pleistocene melting of the continental glaciers that covered much of North America, Fennoscandia, and elsewhere, as well as areas of Antarctica and perhaps part of Greenland. As a result, the eustatic mean sea level has risen about 120 m over the past ~21,000 years. The solid Earth's continuing response (GIA) to the unloading consequently results in a current geocenter velocity of less than 1 mm/yr (Greff-Lefftz, 2000; Klemann and Martinec, 2009). This viscoelastic signal is indistinguishable from the PDMT-induced geocenter velocity observed in many geodetic data sets. To study GIA or measure PDMT alone, their geocenter motion signatures need to be separated in the observations.

The importance of $n = 1$ deformation for GIA has long been recognized (e.g., Farrell, 1972; Peltier, 1974). The correct inclusion of accurate $n = 1$ terms in the sea level equation solver over history may be critical in GIA model predictions, especially for globally averaged quantities such as the GIA correction for altimetric or tide gauge determinations of mean sea level rise. However, because of difficulties associated with the special boundary conditions, the actual implementation of such terms has been slow in the GIA modeling community. And it is not clear if many GIA model predictions of surface velocity include the correct $n = 1$ components.

Currently, most GIA models, although more or less constrained by various data, are largely based on forward-fitting approaches, which contain inherent ambiguities and cannot provide reliable quantitative uncertainty assessments. Consequently, many model predictions may contain unknown but potentially large errors. On the other hand, if any GIA quantities can be uniquely measured, they can be used to improve our understanding of the complex process. Although the geocenter velocity's constraint on GIA is non-unique, it represents the longest wavelength rebound process of

the solid Earth. As such, geocenter velocity may provide the much-needed sensitivity to the deepest part of the mantle allowing us to overcome the current ambiguities in viscosity inference (Paulson et al., 2007) when combined with other data.

On even longer time scales, plate motion, slab subduction, mantle upwelling plumes, and the resulting mantle density heterogeneity will also drive geocenter motion. For example, since oceanic crust is denser than that of the continental crust, isostasy dictates that the latter should have higher columns above the equilibrium depth and thus higher topography. The horizontal movement of topography associated with plate motion will then change the CF. Over time, these slow phenomena can create large offsets, up to hundreds of meters, between CM and CF. When the evolution of the internal load is reasonably inferred from other sources, then these processes may be able to explain a significant bulk of the current static offset between CM and CF. However, these processes are so slow that their contribution to present-day geocenter motion are generally negligible (Greff-Lefftz et al., 2010).

4. Geodetic implications

4.1. Geocenter motion and reference frame

Geocenter motion is an important translational mode of Earth's time-variable shape. Since the long-term mean CM is theoretically defined as the origin of ITRF, geocenter motion naturally enters into the measurement equations of most large-scale geodetic systems and is intimately related to the accuracy and stability of the ITRF origin. Consequently, accurate modeling or determination of geocenter motion at time scales appropriate for the duration of systems' operations will improve the integrity and accuracies of the geodetic solutions. In addition, and as mentioned in the Introduction, the accuracy with which a geodetic system can determine geocenter motion has been recognized as an excellent overall system performance indicator.

Currently, there are two interrelated challenges for a consistent formulation of geocenter motion in the geodetic systems. The first is the desire to have the instantaneous CM as the coordinate origin for most orbit determination procedures while the ITRF origin is at the long-term mean CM. Secondly, even though a consistent formulation does exist (Heflin et al., 1992; Rülke et al., 2008), many geodetic systems do not have sufficient accuracy or the temporal resolution by themselves to actually provide instantaneous geocentric positions. For example, SLR, which currently is the most accurate satellite tracking technique for geocenter motion, still shows a rather large scatter in its geocenter motion time series at sub-annual time scales that most likely reflects system noise (Collilieux et al., 2009). The Z-component is usually the poorest determined by SLR, as well as by other satellite techniques, due to limited tracking from high latitudes and the orbital inclination coverage of the geodetic satellites.

As a result, many low Earth orbiters contain sub-secular trajectory errors due to the difference between the instantaneous CM and the realized ITRF origin having amplitudes of a few mm, and this may be significant depending on the scientific objectives of the orbiter missions. In addition to the continuous improvements to the various geodetic systems, it appears that discrete global coordinate time series in a reference frame with the origin at the nearly instantaneous CM could help to improve this situation. Such time series would combine the strengths of the different observing techniques and provide nearly instantaneous datum information to systems that lack or are weakly sensitive to such information. Another approach is to adopt modelled or predicted geocenter motion from external sources, if reliable information is available. For example, although the post-TOPEX ocean tide models are not perfect, their predicted contributions to geocenter motion are accurate enough to be included in the geodetic data modeling rather than just ignored, a circumstance that is generally true for tidal effects. The situation is less favorable for non-tidal geocenter modeling. However, independently measured or inferred geocenter motion time series of sufficient accuracy are available (see Section 5) and can be used a priori to help improve the orbit determination procedure, similar to existing models for the ground motion of tracking stations.

At the secular time scale, the ITRF origin is defined at the mean CM. Due to measurement errors and model deficiencies, the coordinates and velocities of the ITRF stations and CN contain errors, both random and systematic. A modified description "origin of the realization" inherent in the ITRF coordinate and velocity estimates, is often used to indicate that it could be different from the mean CM due to these errors. The origin (and scale) realization errors (including an epoch offset and a linear drift in time) are quantified by the translations (and scale factor) of the Helmert transformation between the estimated and true station coordinates and velocities. Also, Helmert transformations between different ITRF realizations show closure errors that reflect origin offsets and drifts. These two descriptions, however, are equivalent, since the origin realization errors are the same as the negative values of CN coordinate and velocity errors in the mean CM frame. In this sense, the ability of a particular ITRF solution to determine the geocentric position and velocity of CN is a direct measure of accuracy and stability of its realized origin (Wu et al., 2011).

4.2. Geocenter motion and sea level

Global mean and regional sea levels have significant impacts on societies of the world. The geocentric global MSL rate determined by TOPEX/Jason altimetric missions since 1992 is about 3 mm/yr (e.g., Lemoine et al., 2010). This level of sea level rise is of the same order of magnitude as the GIA-induced geocenter velocity and the suspected present-day ITRF origin drift error. Annual global MSL variations have amplitudes also at the level of a few mm. Therefore, understanding the impact of geocenter motion and improving the stability of the ITRF origin are critical for accurately determining sea level changes and their physical sources.

The regional geocentric sea level rates are significantly affected by any ITRF origin drift error, while the effect on the geocentric global MSL rate is reduced to about 12% of the origin drift in the polar direction and still not entirely negligible (Morel and Willis, 2005). Moreover, altimeters may contain possible biases and drifts, which are monitored and validated by comparisons with tide gauge measurements. The validation procedures may use GNSS (mostly GPS) to convert the locally measured relative sea level rates to geocentric, and thus may be significantly perturbed by any ITRF scale and origin drift errors due to a substantial north–south hemispherical site distribution imbalance or bias (Collilieux and Woppelmann, 2011). Another important sea level signature is the non-uniform sea level fingerprint patterns of melt-runoff water (Mitrovica et al., 2001). To measure and distinguish such subtle patterns is a real challenge that requires a very stable ITRF origin, among other things. Consequently, more consistent and accurate ITRF realizations will be crucial to monitor geocentric global and regional mean sea level rates to an accuracy of 0.1 mm/yr.

The impact of sea level changes on communities is clearly relative to the coastal land. The mechanisms of thermal expansion, salinity change, and non-steric mass additions all affect the oceanic water volume or heights above the crust (Blewitt, 2003). Such relative sea levels are measured via local tide gauges, or deduced from nominally geocentric sea levels using satellite altimetry. The importance of $n = 1$ surface mass variations and their equivalent geocenter motion on the non-steric sea level determination by GRACE has already been discussed and listed in Table 1. Here, to

convert altimeter-measured sea level changes from geocentric to relative, the motion of oceanic crust relative to CM is required. Since the oceanic area has few geodetic sites, such motion might be better determined using geophysical models (Douglas and Peltier, 2002) or inverse approaches that seek to estimate major geophysical processes affecting the ocean floor (Wu et al., 2010b). A primary contributor to the geocentric sea floor movement is subsidence due to GIA (Douglas and Peltier, 2002) with a predicted global mean rate of −0.3 mm/yr for the geocentric geoid height. With the addition of the GRACE gravity data as a technique for improved measurements of surface mass variability, better ocean monitoring capabilities, improvements in geocenter motion determination, and geophysical models, significant progress can be expected in the coming years towards measuring and understanding global mean and regional sea level changes to the level of 0.1 mm/yr.

5. Measurements

The following two subsections are devoted to a review of the direct satellite tracking and inverse methods for estimating geocenter motion at sub-secular time scales. Measurements of secular geocenter motions or geocenter velocities due to PDMT and GIA face unique difficulties and will be discussed separately.

5.1. Translational approaches

Since satellites orbit CM and because geodetic stations are located on the surface of the solid Earth, the feasibility of determining geocenter motion using satellite tracking has long been recognized (Stolz, 1976; Vigue et al., 1992). However, the small amplitude of the geocenter motion, the noise in observational data sets, and uncertainties in background models make such a determination very demanding. The first credible seasonal and tidally coherent geocenter motion determinations were made using LAGEOS satellite laser ranging (Eanes et al., 1997; Watkins and Eanes, 1997; Cheng et al., 2010). With the coordinate origin of the satellite orbit determination system defined at CM, a time series of (e.g., weekly, monthly, or tidally coherent) net translational offsets characterizing the mean motion of the network was introduced into the observation equation of each tracking station and estimated in the solution such as $\mathbf{r}_i(t) - \mathbf{r}_{cm} = \mathbf{T}(t)$. Note that $\mathbf{r}_i(t) - \mathbf{r}_{cm}$ is the incremental geocentric coordinate vector for the ith site. With a variant form reported earlier that also estimates coordinates for non-fiducial stations (Vigue et al., 1992), the method is sometimes referred to as the kinematic approach and has also been applied to geocenter motion measurements using GPS tracking of the GRACE satellites (Kang et al., 2009). With equal weighting of the stations, it can be shown that the estimate is:

$$\hat{\mathbf{T}}(t) = \sum_{i}^{N} \frac{\mathbf{r}_i(t)}{N} - \mathbf{r}_{cm} \tag{20}$$

Apparently, this is an unbiased estimate of the negative of the geocenter motion between CM and CN, despite the fact that no individual site displacement is allowed in the solution.

A fiducial-free transform approach is widely used in GPS solutions (Heflin et al., 1992; Blewitt et al., 1992). This technique estimates every station coordinate component and assigns a large a priori uncertainty of 1 m. The exact relation between the fiducial-free GPS solution and the ITRF coordinates can be written as (e.g., Tregoning and van Dam, 2005):

$$\mathbf{x}_i^{cm} = \bar{\mathbf{X}}_i^{cn} + \boldsymbol{\epsilon}_i^{cn} + \mathbf{A_i}\mathbf{T}, \tag{21}$$

where the epoch fiducial-free coordinates for the ith site $\mathbf{x}_i^{cm}$ are in the CM frame. $\bar{\mathbf{X}}_i^{CN}$ are the ITRF coordinates linearly mapped to the solution epoch for the ith site. At sub-secular time scales, the ITRF coordinates contain no non-linear motion. The realized origin is thus inherent in the constant coordinates of the network and remains fixed relative to the crust, or more precisely, fixed relative to CN. Thus the ITRF is often referred in the literature, as a CN frame for these time scales even though the realized ITRF origin has a constant offset from CN and the frame is CN fixed only in terms of motion, which concerns us here. $\boldsymbol{\epsilon}_i^{cn}$ is the displacement also in the same CN frame. $\mathbf{T}$ is the vector of transformation parameters. $\mathbf{A_i}$ is the site-specific matrix of partial derivatives. Ignoring $\boldsymbol{\epsilon}_i^{cn}$, the similarity (Helmert) transformation parameters are then estimated between $\mathbf{x}$ containing fiducial-free coordinates of all sites $\mathbf{x}_i^{cm}$, and $\bar{\mathbf{X}}$ containing all ITRF coordinates $\bar{\mathbf{X}}_i^{CN}$:

$$\mathbf{x} - \bar{\mathbf{X}} = \mathbf{A}\mathbf{T}, \tag{22}$$

This procedure is often referred to as the network shift approach, which is very similar to the kinematic approach. The ignored $\boldsymbol{\epsilon}_i^{cn}$ has no effect on the estimated transformation parameters if equal weights are used and no scale offset is estimated simultaneously. This is because the sum of $\boldsymbol{\epsilon}_i^{cn}$ vanishes by definition (Tregoning and van Dam, 2005). Estimating a scale offset complicates matters and can result in additional errors not only in the CN–CM measurement but also in the transformed coordinates (Tregoning and van Dam, 2005; Lavallée et al., 2006). Historically, GPS scale (height) information has been considered quite weak in an absolute sense because of intrinsic correlations with local troposphere parameters and with antenna phase corrections (Ge et al., 2005; Cardellach et al., 2007; Schmid et al., 2007). Estimating a scale factor and transforming to the CN frame is equivalent to borrowing the scale information from the ITRF, which is determined independently from SLR and very long baseline interferometry (VLBI) data. The reason for the additional error is that the current ITRF solutions are long-term realizations that use a linear station motion model and are therefore not consistently similar in shape to the near-instantaneous GPS frames that are continuously deformed by loading and other effects. As the GPS system and global loading models improve, such a practice might need to be modified. Similar approaches have been applied to measure geocenter motion using SLR and DORIS tracking of LAGEOS-1 and 2, TOPEX, SPOT satellites (Bouille et al., 2000; Cretaux et al., 2002; Moore and Wang, 2003; Feissel-Vernier et al., 2006; Gobinddass et al., 2009).

A third method is the dynamic approach that uses a reference frame fixed on the surface of the Earth and estimates three $n = 1$ geopotential coefficients at regular intervals (Kar, 1997; Pavlis, 1999; Guo et al., 2008). Because of complications associated with dynamic parameter implementation and the non-inertial frame, it has not been used widely.

The LAGEOS satellites and orbits were designed specifically for high-accuracy geodesy, employing small, dense, simple, passive bodies at altitudes amenable to high-quality dynamic orbit modeling. However, the number of operational SLR ground tracking stations is sparse, poorly distributed geographically, and still primarily restricted to night-time observing. While the DORIS system has excellent geographic distribution, the positioning information is less accurate than SLR and GPS, and the satellites tracked present significant challenges to precise orbit determination (Feissel-Vernier et al., 2006; Gobinddass et al., 2009). Current results indicate that the DORIS geocenter results are noisier and less stable than those of SLR (Gobinddass et al., 2009; Kuzin et al., 2010; Altamimi et al., 2011). The GPS system has the highest station and data density, but complicated surface force modeling, the different blocks of satellite design, tropospheric delay modeling/estimation, and transmitter/receiver phase center calibrations create many complications for geocenter motion determination. Moreover, GPS results are especially sensitive to the empirical orbit parameters

Table 2
Measured and predicted annual geocenter motion.

Studies	x		y		z		Time span
	Amp. (mm)	Phase (day)	Amp. (mm)	Phase (day)	Amp. (mm)	Phase (day)	
SLR KA (Eanes et al., 1997)	2.2	60	3.2	303	2.8	46	1992.7–1997.0
SLR KA (Bouille et al., 2000)	2.1 ± 0.5	48	2.0 ± 0.5	327	3.5 ± 1.5	43	1993.0–1996.8
SLR KA (Cretaux et al., 2002)	2.6 ± 0.5	32 ± 7	2.5 ± 0.1	309 ± 4	3.3 ± 1.0	36 ± 10	1993.0–2000.0
SLR KA (Moore and Wang, 2003)	3.5 ± 0.6	26 ± 10	4.3 ± 0.6	303 ± 8	4.6 ± 0.6	33 ± 7	1993.1–2001.7
SLR KA (Cheng et al., 2010)	3.2 ± 0.4	31 ± 5	2.6 ± 0.4	305 ± 5	4.3 ± 0.3	31 ± 5	2002.0–2010.6
GPS/LEO KA (Kang et al., 2009)	3 ± 0.2	32 ± 14	2.4 ± 0.2	353 ± 14	4.0 ± 0.3	288 ± 16	2003.0–2007.5
GPS NS (Rebischung et al., 2010)	2.9	363	3.2	319	3.0	168	1997.0–2009.0
GPS UA (Lavallée et al., 2006)	2.1 ± 0.2	39 ± 4	3.2 ± 0.1	346 ± 2	3.9 ± 0.2	74 ± 2	1997.2–2004.2
GPS UA (Fritsche et al., 2010)	0.1 ± 0.2	40 ± 93	1.8 ± 0.2	342 ± 11	4.0 ± 0.2	22 ± 6	1994.0–2008.0
INV (Kusche and Schrama, 2005)	3.9	22	2.7	25	7.6	57	1999.5–2004.5
INV (Wu et al., 2006)	1.8 ± 0.4	46 ± 15	2.5 ± 0.3	329 ± 5	3.9 ± 0.4	28 ± 5	2002.3–2004.2
INV (Swenson et al., 2008)	1.5	49	2.6	331	1.5	58	2003.0–2007.0
INV (Wu et al., 2010a)	1.8 ± 0.1	49 ± 4	2.7 ± 0.1	329 ± 2	4.2 ± 0.2	31 ± 3	2002.3–2009.3
INV (Rietbroek et al., in press-a)	2.1	60	3.4	327	2.6	25	2003.0–2009.0
CLM (Dong et al., 1997)	4.2	47	3.2	295	3.5	36	1992.0–1995.0
CLM (Chen et al., 1999)	2.4	26	2.0	0	4.1	43	1992.7–1997.0
CLM (Collilieux et al., 2009)	2.1	28	2.1	342	2.7	49	1993.0–2006.0

The amplitude A^i and phase ϕ^i are defined by $x^i_{cm} - x^i_{cf} = A^i \cos\omega(t - t_0 - \phi^i)$. Since t_0 is usually defined as January 1 of a particular year, ϕ^i also coincides with the annual peak time of the ith coordinate time series. KA: kinematic approach. NS: network shift. UA: unified approach. INV: inverse method. CLM: climate model.

that must be used to account for poorly understood solar radiation pressure effects (Hugentobler et al., 2006). Consequently, credible equatorial geocenter motion time series from GPS and GPS tracking of LEO satellites have emerged only recently (Rebischung and Garayt, 2010; see also Kang et al., 2009 for GPS tracking of low Earth orbiters). With better estimates of transmitter and receiver antenna phase center variations (Haines et al., 2004), more accurate solar radiation pressure models, and better understood and reduced draconitic errors (with a period of 351.2 days for the GPS orbit constellation to repeat its orientation relative to the sun; see Ray et al., 2008), progress is being made to achieve competitive GPS contributions to geocenter motion determination (Weiss et al., 2011). Whether GPS results for the axial geocenter component will attain a high level of accuracy remains to be seen.

An apparent advantage of the satellite tracking methods is that they determine the absolute location of CM with respect to Earth's surface. However, for the purpose of determining the motion between CM and CF or, equivalently, $n = 1$ surface mass variations, a major limitation of the direct satellite methods is that they use their various CNs to approximate CF. Differences between CF and CN (the "network effect") in annual motion depend on surface mass variations and network configurations and can reach 1 mm for a 30-station network (Wu et al., 2002; see also Dong et al., 2002, and Collilieux et al., 2009). Such a problem also complicates a direct comparison of the different techniques. As accuracies of tracking systems improve, a more uniform and denser network geometry is needed to limit the approximation error. Moreover, as we shall see, a unified observation model and incorporation of other data sets can significantly improve geocenter motion results.

5.2. Degree-1 and inverse approaches

Although $n = 1$ deformation has long been known to the geophysical community, the present-day load-induced motion between CE and CF, a function of the $n = 1$ load Love numbers (see (3) and (13)), is very small (about 2% of CM–CF) and has been rightfully disregarded (Dong et al., 1997; Chen et al., 1999). Blewitt et al. (2001), however, recognized the importance and observability of geocenter motion through $n = 1$ deformation by a globally distributed geodetic network. They used (12) in (21) to express $\boldsymbol{\varepsilon}_i^{cn}$ explicitly as functions of $n = 1$ surface mass coefficients. Equation (21) thus becomes a vector observation equation for 3-dimensional displacements measured by the GPS system, which is then used to estimate the $n = 1$ load coefficients and six transformation parameters simultaneously.

However, for spatially limited ground networks, the truncated higher-degree terms in (12) can alias significantly into the estimated $n = 1$ terms (Wu et al., 2002). To overcome such a difficulty, a sufficient number of higher-degree terms must be estimated simultaneously (Blewitt and Clarke, 2003; Wu et al., 2003; Mendes et al., 2006). In this spirit, the $n = 1$ deformation approach really should be an inverse approach. To overcome the problem of heterogeneous GPS site distribution and the severe data sparseness in the oceanic area, various additional data and improved inversion methods have been used. Kusche and Schrama (2005) applied a regularization matrix to constrain the limited oceanic mass variability. Clarke et al. discuss the gravitational self-consistency and "passive" response of the oceans to follow the equilibrium, but time-variable, geoid (Clarke et al., 2005) and demonstrate the method of using land-only basis functions to invert GPS data for the surface load instead of the regular spherical harmonic functions (Clarke et al., 2007).

GRACE gravity data have been incorporated into the GPS inversion to mitigate the aliasing of higher-degree terms (Davis et al., 2004; Munekane, 2007). The method of least squares with reduced a priori information under the platform of singular value decomposition proposed by Matsu'ura and Hirata (1982) has been used by Wu et al. (2006) to combine GPS data with a data-assimilated ocean bottom pressure (OBP) model as well as GRACE data to estimate surface mass variations up to degree and order 50. GRACE gravity data have also been combined with ocean bottom pressure models by Swenson et al. (2008) to derive $n = 1$ surface mass variations and geocenter motion. The information contents of the various data sets in the combinations, technical issues such as GPS data lacking network scale information on sub-secular time scales, and realistic accuracies and data weights have been discussed in detail recently (Jansen et al., 2009; Munekane, 2007; Rietbroek et al., 2009, in press-a).

The inverse approaches that use data combinations generally produce more stable geocenter motion time series with less temporal scatter than the direct satellite results (Figs. 5 and 6). But most of the annual results from the two approaches agree reasonably well with each other and with model predictions (Table 2), especially considering the difference between CN and CF. To mitigate the effect of relative motion between CN and CF, Collilieux et al. (2009) compared model-predicted and inverse-estimated geocenter motion time series between CM and the CN of a particular SLR

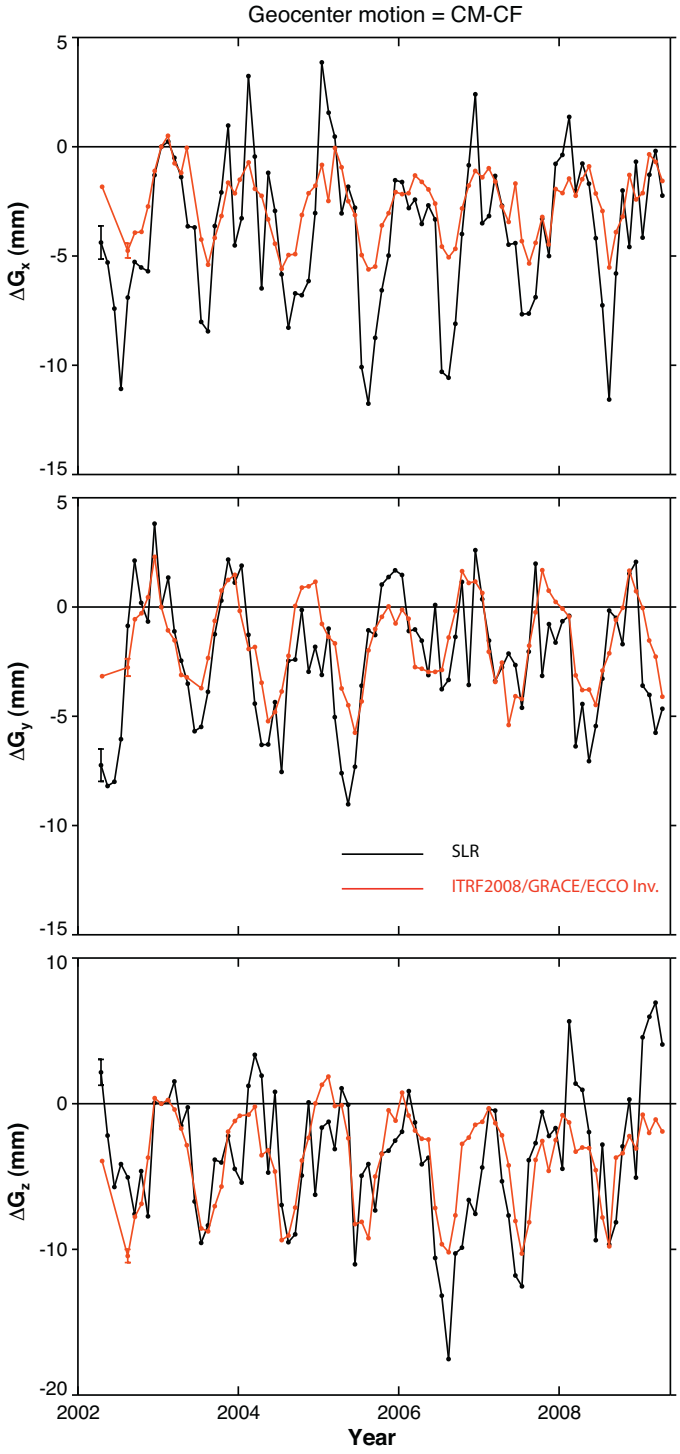

Fig. 5. Comparisons between detrended monthly geocenter motion time series determined from SLR data and the kinematic approach (Black dots, Cheng et al., 2010) and from a combination of ITRF2008 residuals, GRACE, and ECCO OBP data using the inverse approach (red dots, Wu et al., 2010a). All time series are incremented against the respective values of January 2003. $1-\sigma$ error bars are shown only at beginnings of time series.

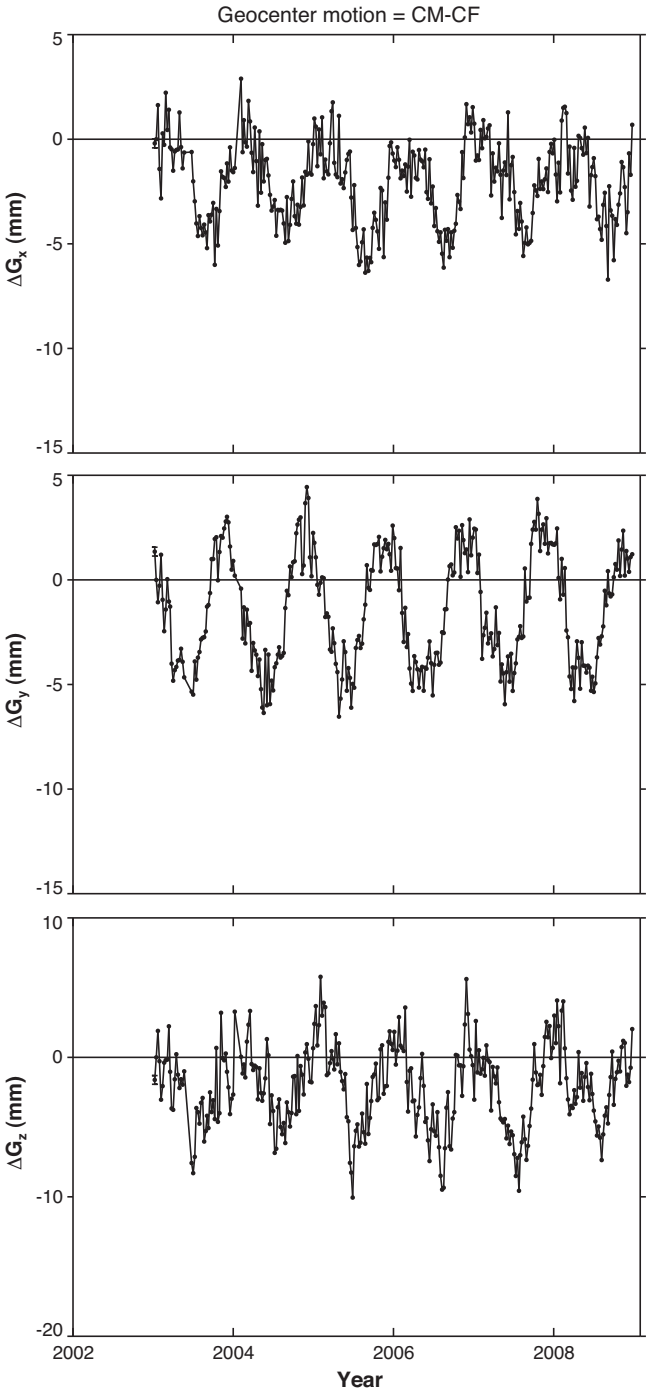

Fig. 6. Detrended weekly geocenter motion time series obtained by inverting a combination of GRACE, GPS, and simulated OBP (using the FESOM model) data. (Adapted from Rietbroek et al., in press-a. Similar to Fig. 5 otherwise.)

network with the direct SLR measurements (Fig. 7). The annual cycles are quite similar despite high noise in the SLR data. As the SLR ground network improves, and the GPS network shift approach becomes more competitive, an optimal approach is to combine the translational and inverse approaches together using the unified observation equations for all ground geodetic measurements (Lavallée et al., 2006; Rülke et al., 2008; Fritsche et al., 2010). Instead of solving for T and $\varepsilon_i^{cn}(\sigma_{nmq})$ in (21) as independent parameters, both should be written as functions of σ_{nmq}, which are then estimated. Recent homogeneously reprocessed GPS data have clearly improved the inverse results. However, to reconcile the remaining differences among solutions, and noting that geocenter motion may vary strongly over time, the issues of further systematic errors in the geodetic data and ocean models as well as the optimal weighting of the data sets should be examined further. The effects of eustatic ocean mass addition and the time-variable equilibrium oceanic geoid on various inversions should also be examined.

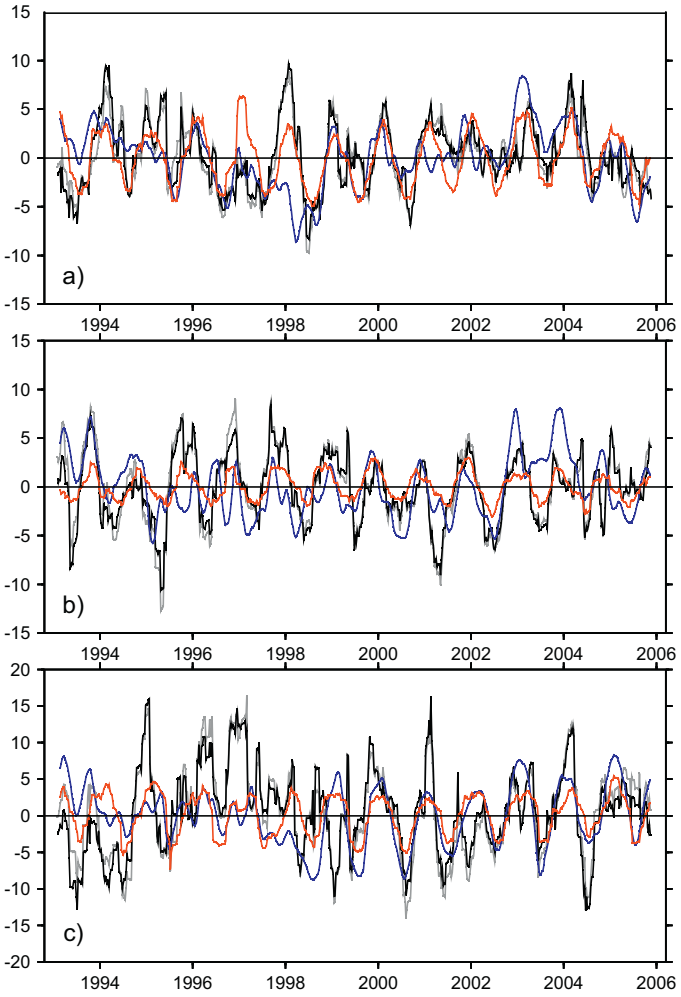

Fig. 7. Estimated geocenter motion time series between CM and CN of the International Laser Ranging Service network with a 10-week running average filter (in mm): a) X-component, b) Y-component, c) Z-component. Black, direct translational determination using SLR data with scale also estimated; gray, direct SLR determination but scale not estimated; blue, inversion of global GPS and ECCO OBP data; red, predicted from a joint geophysical fluid model of atmosphere, oceans and hydrology. Figure from Collilieux et al. (2009).

5.3. Geocenter velocity

Measuring geocenter velocity due to both PDMT and GIA is complicated by several factors. The direct satellite measurement using the time derivative of (20) can only hope to determine the total velocity between CM and CN. But here, differential motion between CF and CN due to other geophysical processes may be considerable. For example, the horizontally moving tectonic plates on Earth's surface do not result in significant geocenter motion. However, if tracking sites are concentrated on one or a few plates, the direct satellite determination will have a sizable apparent motion between CM and CN. Estimating plate and geocenter motion together may largely mitigate this aliasing problem (Argus, 2007). However, the effects of PDMT and GIA on the CF and CN difference have not been quantitatively evaluated. Moreover, the current realized ITRF origin may have a drift error at the level of 1 mm/yr (Altamimi et al., 2007), which, as discussed in the last section, is the same error in CM–CN determination. Note, however, that more recent analysis indicates an ITRF origin uncertainty closer to 0.5 mm/yr (Wu et al., 2011). Errors at this level would limit the usefulness of the direct satellite tracking results, considering that the amplitude of the signal is at the same level. Incidentally, Métvier et al. (2010) have considered the possibility of acceleration in geocenter motion due to accelerated mass losses over polar ice sheets, and concluded that the acceleration is too small to explain the large origin drift between the 2000 and 2005 ITRF realizations.

Inverse approaches to geocenter velocity have the potential to separate the contributions of PDMT and GIA using multiple data sets. GRACE gravity data from $2 \leq n \leq 60$ and two ocean bottom pressure models have been combined to estimate geocenter velocity due to PDMT, after the GIA signatures have been removed from GRACE data using the standard ICE-5G/VM2 model (Swenson et al., 2008). An approximate eustatic correction may have also been applied to the OBP models. As discussed above, the GIA model may contain unknown and potentially large errors. To overcome this difficulty, a global inversion of a combination of GRACE, OBP, and surface velocity data has been carried out to estimate PDMT and GIA signatures simultaneously including their separate contributions to geocenter velocity (Wu et al., 2010b). The kinematic inversion was aided by reduced and dynamically constructed a priori GIA information including a full covariance matrix to exploit the intrinsic relationships among the signatures and to ensure that the inverted coefficients are dynamically consistent. Recently, GRACE and Jason altimetry data have been combined with various models to improve amplitudes of variation patterns described by physical and statistical models (Rietbroek et al., in press-b). The geocenter velocity results are listed in Table 3. In general, the estimated PDMT contributions have the same order of magnitude, but the results depend quite strongly on the different OBP models used in each case and on the altimeter/steric model with significant differences. The agreement on the Z-component of the GIA contribution is particularly encouraging at this early stage of investigation into this rather complex problem, probably due to the fact that the Laurentide deglaciation is the dominant driving force for this phenomenon.

6. Discussion

Similar to Earth rotation (equivalent to $n = 2$ constituents of their mass-driven excitations), geocenter motion and the associated $n = 1$ surface and internal mass variations are among the longest wavelength global change phenomena. As millimeter geodesy becomes a reality, it has become increasingly apparent that the study of geocenter motion is an important and fundamental branch of research in the field of global geodesy. Geocenter motion is also intimately related to the origin of the ITRF, a principal datum for global change monitoring. In addition, since geocenter motions contain signatures from both present-day load changes and GIA signatures, observing these motions to a high precision has significant practical geodetic and geophysical implications for the measurements and interpretations of sea level change, ice mass balance, ice mass history, rheology, and mantle convection. In this section, we discuss the prospects for improving our ability to measure/observe or model geocenter motions.

6.1. Prospects for geodetic measurements

The origin of the ITRF, currently realized using only SLR data, is ideally defined at the long-term mean CM. The ability of the participating geodetic satellite systems (SLR, GNSS, DORIS) to determine geocenter motion is directly related to the accuracy and stability of the realized ITRF origin. To achieve an accurate and stable ITRF for global change monitoring at the level of 0.1 mm/yr, significant improvements must be made to tracking data yields and precision, ground network geometry and density, consistency and accuracy of dynamic and kinematic models, and estimation strategies.

Another issue is that the linear motion model employed by the ITRF prohibits the full exploitation of the combined strengths of

Table 3
Measured and predicted secular geocenter motion in mm/yr.

Studies	Present-day surface mass trend			GIA		
	x	*y*	*z*	*x*	*y*	*z*
GR + ECCO (Swenson et al., 2008)	−0.12 ± 0.04	0.07 ± 0.03	−0.14 ± 0.05			
GR + OMCT (Swenson et al., 2008)	−0.20 ± 0.04	−0.02 ± 0.03	0.06 ± 0.05			
GR + ECCO + SV (Wu et al., 2010b)	−0.08 ± 0.04	0.29 ± 0.05	−0.16 ± 0.07	−0.10 ± 0.01	0.11 ± 0.02	−0.72 ± 0.06
GR + Jason-1 (Rietbroek et al., in press-b)	−0.14	0.12	−0.37	−0.14	0.31	−0.71
ICE-5G/IJ05/VM2				−0.12	0.24	−0.48
ICE-5G/LM+ (Klemann and Martinec, 2009)				−0.13	0.33	−0.80

GR – GRACE data.
ECCO – Data-assimilated OBP model of the consortium for estimating the circulation and climate of the ocean.
OMCT – Simulative OBP model of the ocean model for circulation and tides.
SV – Surface velocities from space geodesy.
ICE-5G – Ice history model (Peltier, 2004).
IJ05 – Ice history model for Antarctica (Ivins and James, 2005).
VM2 – Earth rheology model (Peltier, 2004).
LM+ – A mantle viscosity profile that has a lower-mantle viscosity 20 times larger than that of the upper mantle

the different geodetic techniques at sub-secular time scales, and creates some conceptual difficulties. For continuous global change monitoring by satellite gravity missions, a research version of reference frame realizations with an origin at the nearly instantaneous CM may be useful. The International GNSS Service (IGS) provides a product stream of coordinate time series at weekly intervals in the ITRF frame whose origin is crust-fixed at sub-secular time scales while kinematically extracting the weekly apparent geocenter motion as a Helmert translation. Producing an analogous product based on all four geodetic observing systems (including also VLBI) in a unified geocentric reference frame is much more difficult because inter-system tie measurements are made only infrequently and the tie discrepancies are troublingly large compared to the internal frame precisions. Since the CM is sensed by tracking spacecraft in orbits that are subject to perturbations of numerous forces, the uncertainties in dynamic orbit modeling and antenna phase center biases for GPS and range biases for SLR appear to be the major limiting factors. For geocenter motion and particularly for $n = 1$ surface mass variations, the eventual barrier for the direct satellite method may be the limited ground network geometry and lack of data coverage over the vast oceanic area. In this case, using a unified approach and combining geometric data with OBP/gravity data or models is clearly more desirable.

Reference frame solutions based on SLR observations rely on the geodetic satellites LAGEOS-1 (launched May 1976 at altitude 5850 km), LAGEOS-2 (October 1992 at 5625 km), Etalon 1 (January 1989 at 19,105 km), and Etalon 2 (May 1989 at 19,135 km), with near-circular orbits having inclinations of 109.84°, 52.64°, 65.3°, and 65.2°, respectively (see http://ilrs.gsfc.nasa.gov/). The active, permanent, ground tracking stations number about 43 and are distributed between latitudes +60.2° and −36.8°. Only seven of these tracking stations are located in the southern hemisphere. There is a heavy concentration of sites in Europe and East Asia. The highly non-uniform network distribution is clearly related to a relative weakness in determining axial geocenter motions. Furthermore, the number of observations varies by over nearly two orders of magnitude among the stations, ranging from more than 25,000 normal points per year on LAGEOS from Yarragadee (Australia) to a few hundred. Tracking yields are affected by such factors as the ability to observe during daylight (especially for higher targets), the frequency of cloudless weather (often seasonal), and the power of the laser transmitter. Single-shot ranging RMS values typically fall between 5 and 20 mm, though a few stations are poorer. Uncalibrated station- and target-dependent range biases must be adjusted empirically in the data analysis and remain a major complication for SLR despite the progress made (e.g., Appleby et al., 2008). All these factors, particularly the existing SLR observational heterogeneities, create opportunities for significant systematic biases in the analysis results.

Since 1992, SLR data are normally reduced in weekly batches that rely on well-modelled orbital dynamics to integrate the irregularly and non-uniformly acquired observations into reliable geodetic results. Prior to the launch of LAGEOS-2 in 1992, 15-day analysis arcs were used. The WRMS scatter of weekly SLR station position residuals from the ITRF2008 combination generally falls between 5 and 10 mm per component (Altamimi et al., 2011).

Significant improvements in SLR results will depend on the success of international efforts to rebuild the global network infrastructure with a goal of at least 30 more evenly distributed core stations, each equipped with new generation tracking systems. According to M. Pearlman (private communication 2011), the new systems will operate with "(1) higher repetition rate (100 Hz to 2 kHz) lasers to increase data yield and improve normal point precision; (2) photon-counting detectors to reduce the emitted laser energies by orders of magnitude and reduce optical hazards on the ground and at aircraft (some are totally eye-safe); (3) multi-stop event timers with a resolution of a few picoseconds to improve low energy performance in a high solar-noise environment; and (4) considerably more automation to permit remote and even autonomous operation. Many systems are working at single photon detection levels with Single Photon Avalanche Diode (SPAD) detectors or MicroChannel Plate PhotoMultiplier Tubes (MCP/PMIs). Some systems are experimenting with two-wavelength operations to test atmospheric refraction models and/or to provide unambiguous calibration of the atmospheric delay." As this effort involves considerable expense among a number of different national agencies, the likelihood and schedule for completion is unknown, though upgrades of some existing stations are already underway.

Until now, GNSS results have actually been dominated by GPS data, though GLONASS contributions have been steadily increasing ever since the system was restored about 2008. GNSS constellations from China and Europe are in the offing during the 2010s. GPS consists of up to 31 operational satellites grouped into six orbital planes with inclinations of about 55° at an altitude of about 20,200 km. The GPS ground tracks repeat each sidereal day. GLONASS is fundamentally similar, with at least 24 satellites planned. However, the three GLONASS orbits are lower, about 19,100 km so that their ground tracks repeat only every 8 days. The GLONASS inclinations are also steeper than GPS, about 65°, giving better coverage over high latitudes.

Permanent, continuous GNSS tracking stations are far more numerous than any other geodetic technique with numbers reaching into the many thousands for continuous stations with open data access. The core of several hundred GNSS reference stations coordinated by the IGS are reasonably well distributed over land

areas between latitudes +78.9° and −77.8° but gaps remain over parts of Africa and large oceanic regions, particularly the Pacific. The geometric weaknesses for GNSS monitoring of geocenter motion therefore come mostly from the polar observing gaps in the satellite constellations (70° for GPS; 50° for GLONASS) that impacts the Z-component estimates. In addition, inversions for the $n = 1$ surface mass variations are adversely affected by the large coverage gaps over mostly oceans that necessitates adding modelled ocean bottom pressure information from models (See Section 5.2).

Unlike other techniques, the data yields from GNSS-stations are comparatively uniform and dense, so that random noise is probably insignificant. However, systematic errors, particularly those related to local station equipment configurations and factors such as multipath conditions and winter snowfall, appear to vary greatly among stations. The scatters of the GNSS weekly position residuals derived from ITRF2008 are 1–2 mm in the north and east components and 4–6 mm in vertical (Altamimi et al., 2011). Height estimates are less precise by a factor of 2–3 due to modeling the highly correlated tropospheric propagation effects.

More important than the infrastructure limitations for GNSS are probably the analysis limitations, in particular the modeling of empirical solar radiation pressure parameters. Orbital dynamics for the unwieldy GNSS satellites cannot be modelled accurately a priori without including purely empirical parameters in the estimation. As shown by Hugentobler et al. (2006) and others, there is an inherent coupling between these parameters and long-wavelength signals such as geocenter motion. Another complication is the need to determine calibrations for satellite-transmit antenna-offsets and beam phase patterns from the geodetic data rather than from an independent source. This factor introduces additional undesirable parameter correlations and a direct dependence on the ITRF scale (Schmid et al., 2007). Prospects for improved GNSS results rest largely on the potential for significantly improved dynamical modeling and antenna calibration methods that are highly uncertain. In the mean time, axial geocenter determinations from GNSS will remain less accurate than those from SLR. However, as the surface density of GNSS-stations continues to grow, inversions of $n = 1$ deformations will improve, though possibly only marginally, if the oceanic gaps cannot be filled by many more island installations.

DORIS has tended to produce the least reliable geocenter motion estimates, especially for the Z-component (see Altamimi et al., 2011), despite having the most uniformly distributed tracking network. The tracking station latitude range is the same as for the GNSS network but they number only about 57. The ground spacing is fairly even to minimize interference between the transmit beacons that are observed from receivers deployed onboard a temporally varying mix of remote sensing satellites, such as TOPEX/Poseidon, Jason 1/2, Envisat, Cryosat 2, and the SPOT series 2/3/4/5. These bulky spacecraft, which were not designed for high-accuracy terrestrial geodesy, have low altitudes of 720–1350 km and inclinations of 66° to polar. The evolution of the satellite array is reflected in the WRMS of the ITRF2008 DORIS weekly station position residuals that range from about 10–20 mm per component when 3 or fewer spacecraft have been available to 7–12 mm per component when four or more satellites can be used (Altamimi et al., 2011).

Presumably, the small number of DORIS spacecraft and the difficulties involved in modeling their orbital dynamics are the main limitations of this technique for monitoring geocenter motion. While some progress is likely, results comparable to SLR, or even GNSS, seem remote.

6.2. Status and prospects for global fluid models

As has been established throughout this paper, geocenter motions are driven by the redistribution of atmospheric, oceanic, cryospheric and continental water mass. In addition to the inversion methods described in Section 5.2, the geocenter effects of these temporally varying loads have been forward modelled for more than three decades using different versions of global fluid models (see references presented in the Introduction). A complete and thorough description of each of these models is beyond the scope of this paper. In this section, we will only generally discuss the status of the models and the potential improvements that would affect geocenter modeling.

The largest barrier to forward modeling geocenter variations is the lack of a full system model. A system model should accurately capture the temporal and spatial exchange of fluid mass between all the components of the Earth system and should not allow mass to enter into or escape out of the system, although changes in form are allowed, e.g. ice to liquid water or liquid water to water vapor. Many groups motivated to understand the complex relationships between the components of the Earth's climate system have been pursuing the development of a complete system model. In these models, however, carbon cycling or energy flow between the components as opposed to a fundamental understanding of the mass exchange is goal of the model.

One general circulation model that takes into account how mass changes in the atmosphere and to some extent in continental hydrology affect changes in ocean mass is the Ocean Model for Circulation and Tides (OMCT) (Thomas, 2002). Ocean bottom pressure changes are caused by (1) the internal mass redistribution of the ocean driven by atmospheric circulation; (2) water mass entering or leaving the ocean (e.g. the global water cycle) (Chambers et al., 2004); and (3) a change in the integrated atmospheric mass over the ocean areas (Ponte, 1999). Changes in bottom pressure from OMCT are derived by forcing the ocean model with atmospheric surface fluxes of momentum, heat and freshwater, as well as by atmospheric pressure.

A second model source of ocean bottom pressure is the Estimating the Circulation and Climate of the Ocean (ECCO) model. In this model, ocean bottom pressure are obtained by least squares fitting a general circulation model to as much in situ and satellite data as possible (e.g. Argo floats, altimetry, SST), by adjusting its forcing fields and initial conditions (Wunsch et al., 2009). Proposals for improving the ECCO model stress the importance of including the effects of sea ice and ice sheet melting, thus capturing the mass exchange between three (ice, atmosphere, ocean) of the four fluid components (ice, atmosphere, ocean, continental water) in the Earth system into a single model. When compared with independent data sets, the ECCO model performs better than the OMCT model. This result is expected since ECCO assimilates real data and OMCT uses an atmospheric model as forcing.

Neither OMCT nor ECCO hold ocean mass constant. This is due to the Boussinesq approximation used in the models, i.e. oceanic volume, and not mass, is held constant in the general circulation model. Real long-term variations in OBP do exist due to (1) trends in freshwater fluxes; (2) trends in the atmospheric forcing; (3) real long-term variations in the large-scale circulation; and (4) tectonophysical changes in the ocean bottom level including GIA effects. Unfortunately, there is currently little possibility for determining what fraction of the OMCT and ECCO OBP trends are realistic or not. The biggest improvement in bottom pressure models for geocenter determination would be the ability to hold the total mass constant. Unfortunately, as OBP is generated as a byproduct of these ocean circulation models that do not require mass conservation for precision, it is unlikely that this constraint will be implemented.

In the short term, we can expect improvements in these OBP data to come mostly from improved spatial resolution.

Large-scale hydrological models range between water balance concepts, mainly used for off-line hydrological studies, and energy-balance concepts that describe soil–vegetation–atmosphere

transfers and that are mainly coupled to climate models at different scales. Models belonging to the former category include WBM (Fekete et al., 2002), WGHM Model (Döll et al., 2003). Models in the latter category are VIC and its derivative TOPLATS (Liang et al., 1994; Famiglietti and Wood, 1994). The land surface schemes of general circulation models also belong to this category, e.g. TESSL – the land surface component of ECWMF GCM – (van den Hurk et al., 2000) and the various land surface schemes of GLDAS (Rodell et al., 2004). The codes of LaD (Milly and Schmakin, 2002) and PCR-GLOBWB (Van Beek and Bierkens, 2005) take intermediate positions between the water balance approach and the energy-balance approach to modeling continental water mass. Although this list is not exhaustive, it gives a concise overview of the types of models that are currently being used in global hydrological modeling.

With time, these models have become more physically based and their temporal and spatial resolution has increased. Notwithstanding, the degree of physics and detail still remain important for assessing such models on their suitability for the purpose of mass distribution and transport modeling. Also, the capability to tune such models within realistic and consistent limits and their skill to model mass distribution and transport are important. However, even with considerable tuning, the performance of these models may still be poor (Meigh et al., 1999; Döll et al., 2003). Issues to be considered in improving the models are: (i) the number of processes described (e.g. changes in groundwater storage and ice/snow/glacier mass processes); (ii) input data requirements; (iii) the spatial resolution; and (iv) the temporal resolution.

For modeling the atmospheric mass variations, a global atmospheric model is generally used. Such models are developed and run by national meteorological services in order to perform weather prediction for their area of interest. Only a few global models are available, which are designed for global meteorological analyses. Two well-known global atmospheric models are those run by the European Centre for Medium-Range Weather Forecasts (ECMWF) and by the US National Centre for Environmental Prediction (NCEP). Both models provide the required parameters for modeling atmospheric masses (surface pressure, geopotential height, multi-level temperature and specific humidity) on a 6-hourly basis. There are some significant differences between both models mostly in areas with sparse in-situ observations of atmospheric parameters. These are specifically the polar areas (mainly Antarctica) as well as the large oceans (mainly the Southern oceans). The differences between the two models for a specific epoch can reach up to 1–1.5 hPa RMS in terms of surface pressure.

As with the ocean general circulation models and OBP, surface pressure is a byproduct of atmospheric general circulation models whose main goal is to forecast weather. In fact, the atmospheric general circulation models do not even assimilate ground observations of surface pressure. Thus, there is little hope that the atmospheric modellers will be convinced to improve their atmospheric models for the sake of surface pressure estimates. Perhaps as the atmospheric models are improved to better predict the weather, improvements in surface pressure will follow. For now, the geodetic community must accept the limitations in the precision and accuracy of these models.

Until a system model for mass exchange can be developed for geodetic applications, we will be forced to combine these separate fluid models in the best way that we can, i.e. simulating mass conservation by allowing the volume of the oceans to change.

6.3. Prospects for theoretical developments and routine geocenter monitoring

The theoretical aspects of the $n = 1$ surface mass variations and the resultant geocenter motion for a spherical elastic or viscoelastic Earth are relatively simple. The Love numbers are very well separated and provide a convenient mechanism to describe the $n = 1$ deformation. With a possible exception of core pressure variations at interannual and decadal scales, internal loading generally produces negligible geocenter motion at present. However, historical geocenter motion due to interior density anomalies over a long ($>10^5$ years) period of time can significantly impact the history and current state of the Earth's topography. For such long time scales, the linear viscoelasto-gravitational theory has its limitations (Greff-Lefftz et al., 2010), and a more general theory should be pursued in the future.

Ignoring the small effects of geocenter motion driven by internal loading, surface load variations that are occurring now and those that have occurred in the past drive present-day geocenter motions. As the precision of geocenter motion determinations improves over time, it remains to be seen if the current elastic and viscoelastic Earth model will continue to be adequate to describe the $n = 1$ deformation. A relevant question is whether the seismically inferred elastic Love numbers are accurate enough to be held fixed or if they can be improved with the deformation and other data. At the same time, the current model assumptions should serve as a caveat for the very high accuracies reported in the literature.

The inverse methods with various data combinations seek to determine the incremental changes in $n = 1$ mass distribution or, equivalently, the motion between CM and CF. However, dependence of the methods on the OBP models is apparent, and the qualities of the models are difficult to evaluate. Even though altimetry and in situ data are assimilated into the ECCO model, they do not directly measure OBP. Improved OBP models can lead to more robust estimates of geocenter motion. Moreover, a unified observation model with data combination has the best potential to provide the highest accuracy geocenter motion time series, especially if systematic errors are understood and reduced in the data sets. Current inverse models assume that Earth's changing shape is caused by surface loading and unloading. While this seems to produce satisfactory global patterns with carefully selected geodetic sites when compared with GRACE gravity observations, any additional mechanisms with significant effects should be included in the future. The estimated geocenter velocity components due to PDMT depend strongly on the OBP model used. However, the magnitudes appear to be limited. The kinematically inverted GIA-induced geocenter velocity components are very precise and do not depend strongly on models except the horizontal extent of historic deglaciation. The physical meaning of the kinematic estimates, however, remains ambiguous and can only be unraveled by dynamic studies in the future. When combined with other data, these components may provide global large-scale constraints on deglaciation history and a unique opportunity to help probe the deep mantle for its rheology.

7. Conclusions

The horizontal transport of ocean, atmospheric, ice, and continental water at the degree-1 spatial scale, induces degree-1 deformation of the solid Earth surface and drives geocenter motion between the center-of-mass of the total Earth system and the center-of-figure of the solid Earth surface. Earth-based tracking of Earth orbiting satellites allows us to observe geocenter motion. These short- and long-term observations of the geocenter are important for climate change modeling including sea level change, present-day ice mass changes, and changes in continental hydrology. However, there are times when we would like to remove the geocenter motion from our observations. In particular, having access to a nearly instantaneous geocenter is extremely important for those missions that can sense geocenter motions to some extent but are not good enough to measure it well independently.

Satellites such as GRACE and satellite altimeters are probably most relevant in this respect. For GPS, which is not as capable of measuring the Z-component geocenter variations, adopting a reliable annual model for the Z-component could be extremely valuable for improving the ITRF. Despite the progress in observing technology and innovative approaches to data modeling, we are still a long way from constraining instantaneous geocenter motion to sufficient precision for either climate modeling or geodetic applications. Prospects for modeling geocenter motion at seasonal and longer periods are much brighter.

Acknowledgements

Part of this work was carried out at the Jet Propulsion Laboratory (JPL), California Institute of Technology, under a contract with the National Aeronautics and Space Administration (NASA), and funded through NASA's International Polar Year and GRACE Science Team programs. We thank Minkang Cheng, Xavier Collilieux, Volker Klemann, John Ries, Paul Tregoning, and Roelof Rietbroek for providing materials from their publications or research. XW thanks Edward Sewall of JPL for editorial help. Constructive suggestions and comments from reviewers and editors are very helpful.

References

Altamimi, Z., Collilieux, X., Legrand, J., Garayt, B., Boucher, C., 2007. ITRF2005: a new release of the international terrestrial reference frame based on time series of station positions and earth orientation parameters. J. Geophys. Res. 112, B09401, doi:10.1029/2007JB004949.

Altamimi, Z., Collilieux, X., Métivier, L., 2011. ITRF2008: an improved solution of the international terrestrial reference frame. J. Geod. 85 (8), 457–473, doi:10.1007/s00190-011-0444-4.

Appleby, G., Wilkinson, M., Luceri, V., Gibbs, P., Smith, V., 2008. Attempts to separate apparent observational range bias from true geodetic signals. In: 16th International Laser Workshop, Poznan, Poland.

Argus, D.F., 2007. Defining the translational velocity of the reference frame of Earth. Geophys. J. Int. 169 (3), 830–838.

Blewitt, G., Heflin, M.B., Webb, F.H., Lindqwister, U.J., Malla, R.P., 1992. Global coordinates with centimeter accuracy in the international terrestrial reference frame using GPS. Geophys. Res. Lett. 19 (9), 853–856.

Blewitt, G., Lavallée, D., Clarke, P., Nurutdinov, K., 2001. A new global mode of Earth deformation: seasonal cycle detected. Science 294 (5550), 2342–2345.

Blewitt, G., 2003. Self-consistency in reference frames, geocenter definition, and surface loading of the solid Earth. J. Geophys. Res. 108 (B2), doi:10.1029/2002JB002290, Art. No. 2103.

Blewitt, G., Clarke, P., 2003. Inversion of Earth's changing shape to weigh sea level in static equilibrium with surface mass redistribution. J. Geophys. Res. 108 (B6), doi:10.1029/2002JB002290, Art. No. 2311.

Bouille, F., Cazenave, A., Lemoine, J.M., Cretaux, J.F., 2000. Geocenter motion from the DORIS space system and laser data on Lageos satellites: comparison with surface loading data. Geophys. J. Int. 143, 71–82.

Cardellach, E., Elósegui, P., Davis, J.L., 2007. Global distortion of GPS networks associated with satellite antenna model errors. J. Geophys. Res. 112, B07405, doi:10.1029/2006JB004675.

Chambers, D.P., Wahr, J., Nerem, R.S., 2004. Preliminary observations of global ocean mass variations with GRACE. Geophys. Res. Lett. 31 (13), L13310.

Chen, J.L., Wilson, C.R., Eanes, R.J., Nerem, R.S., 1999. Geophysical interpretation of observed geocenter variations. J. Geophys. Res. 104 (B2), 2683–2690.

Cheng, M., Ries, J., Tapley, B., 2010. Geocenter variations from analysis of SLR data. In: IAG Commission 1 Symposium 2010, Reference Frames for Applications in Geosciences (REFAG2010), Marne-La-Vallée, France, 4-8 October.

Clarke, P.J., Lavallée, D.A., Blewitt, G., van Dam, T.M., Wahr, J.M., 2005. Effect of gravitational consistency and mass conservation on seasonal surface mass loading models. Geophys. Res. Lett. 32, L08306, doi:10.1029/2005GL022441.

Clarke, P.J., Lavallée, D.A., Blewitt, G., van Dam, T., 2007. Basis functions for the consistent and accurate representation of surface mass loading. Geophys. J. Int. 171, 1–10, doi:10.1111/j.1365-246X.2007.03493.x.

Collilieux, X., Altamimi, Z., Ray, J., van Dam, T., Wu, X., 2009. Effect of the satellite laser ranging network distribution on geocenter motion estimation. J. Geophys. Res. 114, Art. No. B04402.

Collilieux, X., Woppelmann, G., 2011. Global sea-level rise and its relation to the terrestrial reference frame. J. Geod. 85 (1), 9–22, doi:10.1007/s00190-010-0412-4.

Cretaux, J.F., Soudarin, L., Davidson, F.J.M., Gennero, M.C., Berge-Nguyen, M., Cazenave, A., 2002. Seasonal and interannual geocenter motion from SLR and DORIS measurements: comparison with surface loading data. J. Geophys. Res. 107 (B12), Art. No. 2374.

Davis, J.L., Elosequi, P., Mitrovica, J.X., Tamisiea, M.E., 2004. Climate-driven deformation of the solid Earth from GRACE and GPS. Geophys. Res. Lett. 31 (24), Art. No. L24605.

de Viron, O., Schwarzbaum, G., Lott, F., Dehant, V., 2005. Diurnal and subdiurnal effects of the atmosphere on the Earth rotation and geocenter motion. J. Geophys. Res. 110, B11404, doi:10.1029/2005JB003761.

Döll, P., Kaspar, F., Lehner, B., 2003. A global hydrological model for deriving water availability indicators: model tuning and validation. J. Hydrol. 270 (1–2), 105–134.

Dong, D., Dickey, J.O., Chao, Y., Cheng, M.K., 1997. Geocenter variations caused by atmosphere, ocean and surface ground water. Geophys. Res. Lett. 24 (15), 1867–1870.

Dong, D., Fang, P., Bock, Y., Cheng, M.K., Miyazaki, S., 2002. Anatomy of apparent seasonal variations from GPS-derived site position time series. J. Geophys. Res. 107 (B4), 2075, doi:10.1029/2001JB000573.

Dong, D., Yunck, T., Heflin, M., 2003. Origin of the international terrestrial reference frame. J. Geophys. Res. 108 (B4), Art. No. 2200.

Douglas, B.C., Peltier, W.R., 2002. The puzzle of global sea-level rise. Phys. Today 55 (3), 35–40.

Eanes, R.J., Kar, S., Bettadapur, S.V., Watkins, M.M., 1997. Low-frequency geocenter motion determined from SLR tracking (abstract). EOS 78(46), Fall Meet. Suppl., F146.

Famiglietti, J.S., Wood, E.F., 1994. Multiscale modelling of spatially variable water and energy balance processes. Water Resour. Res. 30 (11), 3061–3078.

Farrell, W.E., 1972. Deformation of the Earth by surface loads. Rev. Geophys. 10, 761–797.

Feissel-Vernier, M., Le Bail, K., Berio, P., Coulot, D., Ramillien, G., Valette, J.-J., 2006. Geocentre motion measured with DORIS and SLR, and predicted by geophysical models. J. Geod. 80 (8–11), 637–648, doi:10.1007/s00190-006-0079-z.

Fekete, B.M., Vörösmarty, C.J., Grabs, W., 2002. High-resolution fields of global runoff combining observed river discharge and simulated water balances. Global Biogeochem. Cycles 16 (3), 15.

Fritsche, M., Dietrich, R., Rülke, A., Rothacher, M., Steigenberger, P., 2010. Low-degree earthdeformation from reprocessed GPS observations. GPS Solut. 14, 165–175, doi:10.1007/s10291-009-0130-7.

Ge, M., Gendt, G., Dick, G., Zhang, F.P., Reigber, C., 2005. Impact of GPS satellite antenna offsets on scale changes in global network solutions. Geophys. Res. Lett. 32, L06310, doi:10.1029/2004GL022224.

Gobinddass, M.L., et al., 2009. Improving DORIS geocenter time series using an empirical rescaling of solar radiation 4pressure models. Adv. Space Res. 44 (11), 1279–1287, doi:10.1016/j.asr.2009.08.04.

Greff-Lefftz, M., Legros, H., 1997. Some remarks about the degree-one deformation of the Earth. Geophys. J. Int. 131 (3), 699–723.

Greff-Lefftz, M., 2000. Secular variation of the geocenter. J. Geophys. Res. 105 (B11), 25685–25692.

Greff-Lefftz, M., Legros, H., 2007. Fluid core dynamics and degree-one deformations: Slichter mode and geocenter motions. Phys. Earth Planet. Int. 161, 150–160.

Greff-Lefftz, M., Metivier, L., Besse, J., 2010. Dynamic mantle density heterogeneities and global geodetic observables. Geophys. J. Int. 180, 1080–1094.

Guo, J., Han, Y., Hwang, C., 2008. Analysis on motion of Earth's center of mass observed with CHAMP mission. Sci. China Ser. G 51 (10), 1597–1606.

Haines, B., Bar-Sever, Y., Bertiger, W., Desai, S., Willis, P., 2004. One-centimeter orbit determination for Jason-1: new GPS-based strategies. Mar. Geod. 27, 299–318.

Han, D., Wahr, J., 1995. The viscoelastic relaxation of a realistically stratified earth, and a further analysis of postglacial rebound. Geophys. J. Int. 120, 287–311.

Heflin, M., et al., 1992. Global geodesy using GPS without fiducial sites. Geophys. Res. Lett. 19, 131–134.

Hinderer, J., Crossley, D., Jensen, O., 1995. A search for the Slichter triplet in superconducting gravimeter data. Phys. Earth Planet. Int. 90, 183–195.

Hugentobler, U., van der Marel, H., Springer, T., 2006. Identification and mitigation of GNSS errors. In: Springer, T., Gendt, G., Dow, J.M. (Eds.), Proceedings of IGS Workshop 2006. Darmstadt, Germany, Available electronically at ftp://igscb.jpl.nasa.gov/pub/resource/pubs/06_darmstadt/IGS WS 2006 Papers PDF/11_PP_IGS06_erro_hugentobler.pdf.

Ivins, E.R., James, T.S., 2005. Antarctic glacial isostatic adjustment: a new assessment. Antarct. Sci. 17, 537–549, doi:10.1017/S0954102005002968.

Jansen, M.J.F., Gunter, B.C., Kusche, J., 2009. The impact of GRACE, GPS and OBP data on estimates of global mass redistribution. Geophys. J. Int. 177, 1–13.

Kang, Z.G., Tapley, B., Chen, J.L., Ries, J., Bettadpur, S., 2009. Geocenter variations derived from GPS tracking of the GRACE satellites. J. Geoid. 83 (10), 895–901.

Kar, S., 1997. Long-period variations in the geocenter observed from laser tracking of multiple earth satellites. CSR Report CSR-97-2. Center for Space Research, The University of Texas at Austin, Austin.

Klemann, V., Martinec, Z., 2009. Contribution of glacial-isostatic adjustment to the geocenter motion. Tectonophysics 511, 99–108, doi:10.1016/j.tecto.2009.08.031, 2011 (2009 online first).

Kusche, J., Schrama, E.J.O., 2005. Surface mass redistribution inversion from global GPS deformation and GRACE gravity data. J. Geophys. Res. 110, B09409, doi:10.1029/2004JB003556.

Kuzin, S.P., Tatevian, S.K., Valeev, S.G., Fashutdinova, V.A., 2010. Studies of the geocenter motion using 16-years DORIS data. Adv. Space Res. 46 (10), 1292–1298.

Lambeck, K., 1988. Geophysical Geodesy. Oxford University Press, New York, 718 pp.

Lavallée, D.A., van Dam, T., Blewitt, G., Clarke, P.J., 2006. Geocenter motions from GPS: a unified observation model. J. Geophys. Res. 111 (B5), Art. No. B05405.

Lemoine, F.G., et al., 2010. Towards development of a consistent orbit series for TOPEX, Jason-1, and Jason-2. Adv. Space Res. 46 (12), 1513–1540.
Liang, X., Lettenmaier, D.P., Wood, E.F., Burges, S.J., 1994. A simple hydrologically based model of land surface water and energy fluxes for GSMs. J. Geophys. Res. 99 (D7), 14415–14428.
Matsu'ura, M., Hirata, N., 1982. Generalized least-squares solutions to quasilinear inverse problems with apriori information. J. Phys. Earth 30, 451–468.
Meigh, J.R., McKenzie, A.A., Sene, K.J., 1999. A grid-based approach to water scarcity estimates for eastern and southern Africa. Water Resour. Manag. 13 (2), 85–115.
Mendes, C.P.J., Hobiger, T., Weber, R., Schuh, H., 2006. Spatial spectral inversion of the changing geometry of the Earth from SOPAC GPS data. In: Tregoning, P., Rizos, C. (Eds.), Dynamic Planet: Proceedings of IAG Symposium, vol. 130. Springer, Berlin, pp. 194–201.
Métvier, L., Greff-Lefftz, M., Altamimi, Z., 2010. On secular geocenter motion: the impact of climate changes. Earth Planet. Sci. Lett. 296, 360–366.
Milly, P.C.M., Schmakin, A.B., 2002. Global modelling of land water and energy balances. Part I: the land dynamics (LaD) model. J. Hydrometeorol. 3 (3), 283–299.
Mitrovica, J.X., Tamisiea, M.E., Davis, J.L., Milne, G.A., 2001. Recent mass balance of polar ice sheets inferred from patterns of global sea-level change. Nature 409, 1026–1029.
Moore, P., Wang, J., 2003. Geocentre variation from laser tracking of LAGEOS1/2 and loading data. Adv. Space Res. 31, 1927–1933, doi:10.1016/S0273-1177(03)00170-4.
Morel, L., Willis, P., 2005. Terrestrial reference frame effects on global sea level rise determination from TOPEX/Poseidon altimetric data. Adv. Space Res. 36 (3), 358–368, doi:10.1016/j.asr.2005.05.113.
Munekane, H., 2007. Ocean mass variations from GRACE and tsunami gauges. J. Geophys. Res. 112, B07403, doi:10.1029/2006JB004618.
Pavlis, E.C., 1999. Fortnightly resolution geocenter series: a combined analysis of Lageos 1 and 2 SLR data (1993-1996). In: Ray, J. (Ed.), IERS Analysis Campaign to Investigate Motions of the Geocenter. IERS Technical Note 25. Central Bureau of IERS, Paris, France, pp. 75–84.
Paulson, A., Zhong, S., Wahr, J., 2007. Inference of mantle viscosity from GRACE and relative sea level data. Geophys. J. Int. 171, 497–508.
Peltier, W.R., 1974. The impulse response of a Maxwell Earth. Rev. Geophys. Space Phys. 12, 649–669.
Peltier, W.R., 2004. Global glacial isostasy and the surface of the ice-age Earth: the ICE-5G (VM2) model and GRACE. Ann. Rev. Earth Planet. Sci. 32, 111–149, 2004.
Petit, G., Luzum, B. (Eds.), 2010. IERS Conventions (2010), IERS Technical Note 36. Verlag des Bundesamts für Kartographie und Geodäsie, Frankfurt am Main, 179 pp.
Ponte, R.M., 1999. A preliminary model study of the large-scale seasonal cycle in bottom pressure over the global ocean. J. Geophys. Res. 104, doi:10.1029/1998JC900028.
Ray, R.D., Ponte, R.M., 2003. Barometric tides from ECMWF operational analyses. Ann. Geophys. 21 (8), 1897–1910, doi:10.5194/angeo-21-1897-2003.
Ray, J. (Ed.), 1999. IERS Analysis Campaign to Investigate Motions of the Geocenter. IERS Technical Note 25. Central Bureau of IERS, Paris, France, p. 121.
Ray, J., Altamimi, Z., Collilieux, X., van Dam, T., 2008. Anomalous harmonics in the spectra of GPS position estimates. GPS Solut. 12, 55–64, doi:10.1007/s10291-007-0067-7.
Rebischung, P., Garayt, B., 2010. Recent results from the IGS terrestrial frame combinations. In: IAG Commission 1 Symposium 2010, Reference Frames for Applications in Geosciences (REFAG2010), Marne-La-Vallée, France, 4-8 October 2010.
Rietbroek, R., 2009. Changes in total ocean mass derived from GRACE, GPS, and ocean modelling with weekly resolution. J. Geophys. Res. 114, Art. No. C11004.
Rietbroek, R., et al., in press-a. Global surface mass from a new combination of GRACE, modelled OBP and reprocessed GPS data. J. Geodyn., in press, doi:10.1016/j.jog.2011.02.003.
Rietbroek, R., Brunnabend, S.-E., Schröter, J., Kusche, J., in press-b. Resolving ice sheet mass balance by fitting fingerprints to GRACE and altimetry. J. Geodyn., in press, doi:10.1016/j.jog.2011.06.007.
Rodell, M., Houser, P.R., Jambor, U., Gottschalck, J., Mitchell, K., Meng, C.-J., Arsenault, K., Cosgrove, B., Radakovich, J., Bosilovich, M., Entin, J.K., Walker, J.P., Lohmann, D., Toll, D., 2004. The global land data assimilation system. Bull. Am. Meteor. Soc. 85 (3), 381–394.
Rodell, M., Chao, B.F., Au, A.Y., Kimball, J.S., McDonald, K.C., 2005. Global biomass variation and its geodynamic effects: 1982-98. Earth Interact. 9 (2), 1–19.
Rülke, A., Dietrich, R., Fritsche, M., Rothacher, M., Steigenberger, P., 2008. Realization of the terrestrial reference system by a reprocessed global GPS network. J. Geophys. Res. 113, B08403, doi:10.1029/2007JB005231.
Scherneck, H.-G., Johansson, J.M., Webb, F.H., 2000. Ocean loading tides in GPS and rapid variations of the frame origin. Geodesy 2000 – The Challenges in the First Decade, Vol. 121. Schwarz, Springer, Verlag Berlin Heidelberg.
Schmid, R., Steigenberger, P., Gendt, G., Ge, M., Rothacher, M., 2007. Generation of a consistent absolute phase center correction model for GPS receiver and satellite antennas. J. Geod. 81 (12), 781–798, doi:10.1007/s00190-007-0148-y.
Smylie, D.E., Hinderer, J., Richter, B., Ducarme, B., 1993. The product spectra of gravity and barometric pressure in Europe. Phys. Earth Planet. Int. 80, 135–157.
Stolz, A., 1976. Changes in position of geocenter due to seasonal-variations in air mass and ground-water. Geophys. J. R. Astro. Soc. 44 (1), 19–26.
Swenson, S., Chambers, D., Wahr, J., 2008. Estimating geocenter variations from a combination of GRACE and ocean model output. J. Geophys. Res. 113 (B8), Art. No. B08410.
Tapley, B.D., Bettadpur, S., Ries, J.C., Thompson, P.F., Watkins, M.M., 2004. GRACE measurements of mass variability in the Earth system. Science 305 (5683), 503–505.
Thomas, M., 2002. Ocean induced variations of Earth's rotation – results from a simultaneous model of global circulation and tides. PhD dissertation. University of Hamburg, Germany, 129 pp.
Tregoning, P., van Dam, T., 2005. Effects of atmospheric pressure loading and seven-parameter transformations on estimates of geocenter motion and station heights from space geodetic observations. J. Geophys. Res. 110 (B3), doi:10.1029/2004JB003334, Art. No. B03408.
Trupin, A.S., Meier, M.F., Wahr, J.M., 1992. Effects of melting glaciers on the Earth's rotation and gravitational field: 1965-1984. Geophys. J. Int. 108, 1–15.
Vermeersen, L.L.A., Sabadini, R., Spada, G., 1996. Compressible rotational deformation. Geophys. J. Int. 126, 735–761.
Van Beek, R. Bierkens, M.F.P., 2005. Influence of the quality of climate input on the performance of a MHM for several large catchments. Geophysical Research Abstracts 7, EHGU 05-A-05173.
van den Hurk, B.J.J.M., Viterbo, P., Beljaars, A.C.M., Betts, A.K., 2000. Offline validation of the ERA-40 surface scheme. ECMWF Tech. Memo 295, 42.
Vigue, Y., Lichten, S.M., Blewitt, G., Heflin, M.B., Malla, R.P., 1992. Precise determination of earths center of mass using measurements from the Global Positioning System. Geophys. Res. Lett. 19 (14), 1487–1490.
Wahr, J.M., Molenaar, M., Bryan, F., 1998. Time variability of the Earth's gravity field: hydrological and oceanic effects and their possible detection using GRACE. J. Geophys. Res. 103, 30205–30229.
Watkins, M.M., Eanes, R.J., 1997. Observations of tidally coherent diurnal and semidiurnal variations in the geocenter. Geophys. Res. Lett. 24 (17), 2231–2234.
Weiss, J., Bertiger, W., Desai, S., Haines, B., Harvey, N., 2011. Terrestrial reference frame realization from combined GPS/LEO orbit determination. Geophysical Res. Abstr. 13, EGU2011.
Wu, P., 1978. The response of a Maxwell earth to applied surface mass loads: glacial isostatic adjustment. MSc. Thesis. University of Toronto.
Wu, X.P., Argus, D.F., Heflin, M.B., Ivins, E.R., Webb, F.H., 2002. Site distribution and aliasing effects in the inversion for load coefficients and geocenter motion from GPS data. Geophys. Res. Lett. 29 (24), Art. No. 2210.
Wu, X.P., Heflin, M.B., Ivins, E.R., Argus, D.F., Webb, F.H., 2003. Large-scale global surface mass variations inferred from GPS measurements of load-induced deformation. Geophys. Res. Lett. 30 (14), Art. No. 1742.
Wu, X., Heflin, M.B., Ivins, E.R., Fukumori, I., 2006. Seasonal and interannual global surface mass variations from multisatellite geodetic data. J. Geophys. Res. 111 (B9), Art. No. B09401.
Wu, X., Collilieux, X., Altamimi, Z., 2010a. Data sets and inverse strategies for global surface mass variations. Geophy. Res. Abstr. 12, EGU2010.
Wu, X., et al., 2010b. Simultaneous estimation of global present-day water transport and glacial isostatic adjustment. Nat. Geosci. 3, 642–646.
Wu, X., Collilieux, X., Altamimi, Z., Vermeersen, B.L.A., Gross, R., Fukumori, I., 2011. Accuracy of the international terrestrial reference frame origin and Earth expansion. Geophys. Res. Lett. 38, L13304, doi:10.1029/2011GL047450.
Wunsch, C., Heimbach, P., Ponte, R.M., Fukumori, I., 2009. The global general circulation of the oceans estimated by the ECCO-consortium. Oceanography 22, 88–103.
Zumberge, J., Heflin, M., Jefferson, D., Watkins, M., Webb, F., 1997. Precise point positioning for the efficient and robust analysis of GPS data from large networks. J. Geophys. Res. 102, 5005–5017.